

# Warp Bridge Sampling: The Next Generation

Lazhi Wang and Xiao-Li Meng\*  
 Department of Statistics, Harvard University

October 26, 2021

## Abstract

Bridge sampling is an effective Monte Carlo method for estimating the ratio of normalizing constants of two probability densities, a routine computational problem in statistics, physics, chemistry, etc. The Monte Carlo error of the bridge sampling estimator is determined by the amount of overlap between the two densities. Complementing and generalizing the Warp-I, II, and III transformations (Meng and Schilling, 2002), which are most effective for increasing the overlap between two uni-modal densities, we introduce Warp-U transformations that aim to transform multi-modal densities into *Unimodal* ones but without altering their normalizing constants. The construction of Warp-U transformation starts with a Gaussian (or other convenient) mixture distribution  $\phi_{\text{mix}}$  that has a reasonable overlap with a target density  $p$  underlying the unknown normalizing constant. The stochastic transformation that maps  $\phi_{\text{mix}}$  back to its generating distribution  $\mathcal{N}(0, 1)$  is then applied to  $p$ , resulting in its Warp-U transformation  $\tilde{p}$ . The overlap between  $\tilde{p}$  and  $\mathcal{N}(0, 1)$  is theoretically guaranteed to be no less than the overlap between  $p$  and  $\phi_{\text{mix}}$ , as measured by any  $f$ -divergence, leading to statistically more efficient bridge sampling estimators. We propose a computationally efficient method to find an appropriate  $\phi_{\text{mix}}$ , and use simulations to explore various estimation strategies and the choices of tuning parameters, with the aim to achieve statistical efficiency without unduly losing computational efficiency. We illustrate our findings using 10-50 dimensional highly irregular multi-modal densities. We also propose a strategy for using Warp-U transformations to improve MCMC algorithms, especially for sampling from multi-modal distributions.

*Keywords:* Bridge sampling; Monte Carlo integration; Normal mixture; Stochastic transformation; Normalizing constants;  $f$ -divergence

## 1 Motivations and Applications

As is well known, MCMC methods, such as the Metropolis-Hastings algorithm, enable us to simulate from an unnormalized density without knowing its normalizing constant. However, in many scientific and statistical studies, the very quantity of interest is a normalizing constant, or a ratio of them, as discussed in many articles and books, e.g., Meng and Wong (1996), Gelman and Meng (1998), Shao and Ibrahim (2000), and Tan (2013). Below are a few key applications.

An example from physics and chemistry is the partition function, which describes the statistical properties of a system in thermodynamic equilibrium. It is the integral of the unnormalized

---

\*The paper is a part of the first author's Ph.D. thesis, under the supervision of the second. They gratefully acknowledge helpful conversations with members of the Department of Statistics at Harvard, constructive comments from the audience (especially Christian Robert) of 2016 MCQMC conference at Stanford University, and partial financial support from NSF and JTF. For correspondences, email meng@stat.harvard.edu.

system density  $q(\omega; T, v) = \exp\{-H(\omega, v)/(kT)\}$ , where  $T$  is the temperature,  $k$  is the Boltzmann's constant,  $v$  is a vector of system characteristics, and  $H(\omega, v)$  is the energy function. Because of the high dimensionality of the energy function, Monte Carlo (MC) methods are often the only feasible tool for estimating the partition function, i.e., the normalizing constant of  $q$ ; see, for example, Bennett (1976), Voter and Doll (1985), and Ceperley (1995).

Another example is the computation of the observed-data likelihood,  $L(\Theta; Y_{\text{obs}})$ . More specifically,  $L(\Theta; Y_{\text{obs}})$  is the normalizing constant of the conditional distribution of  $Y_{\text{mis}}$  given  $(Y_{\text{obs}}, \Theta)$ ,  $P(Y_{\text{obs}}|Y_{\text{mis}}, \Theta)$ , with the complete-data distribution as an unnormalized density, i.e.,

$$L(\Theta; Y_{\text{obs}}) \triangleq P(Y_{\text{obs}}|\Theta) = \int P(Y_{\text{mis}}, Y_{\text{obs}}|\Theta) \mathbf{u}(dY_{\text{mis}}),$$

where  $\mathbf{u}$  is the underlying measure (e.g., Lebesgue or a counting measure). As an example in genetics,  $\Theta$  represents the locations of disease genes relative to a set of markers,  $Y_{\text{obs}}$  is a vector of genotypes of markers for some members of a pedigree, and  $Y_{\text{mis}}$  represents unobserved allele types inherited from parents. For a large pedigree with many loci, direct calculation of the observed-data likelihood is often prohibitive. Fortunately, it is feasible to evaluate  $P(Y_{\text{obs}}, Y_{\text{mis}}|\Theta)$  and to simulate  $Y_{\text{mis}}$  from the conditional distribution,  $P(Y_{\text{mis}}|Y_{\text{obs}}, \Theta)$ ; therefore estimating  $L(\Theta; Y_{\text{obs}})$  becomes estimating the normalizing constant of  $P(Y_{\text{mis}}|Y_{\text{obs}}, \Theta) \propto P(Y_{\text{mis}}, Y_{\text{obs}}|\Theta)$ .

In addition, MC integration is often used to estimate Bayes factors. Specifically, let  $Y$  be our data, fitted to two plausible models  $M_0$  and  $M_1$ , parameterized by  $\Theta_0$  and  $\Theta_1$ . The Bayes factor is then the ratio of the model likelihoods,  $P(Y|M_0)$  and  $P(Y|M_1)$ , where

$$P(Y|M_i) = \int P(Y|\Theta_i, M_i)P(\Theta_i|M_i)\mathbf{u}(d\Theta_i)$$

is the normalizing constant of the unnormalized density,  $P(\Theta_i, Y|M_i)$ , of  $\Theta_i$ . In most applications, MC draws of  $\Theta_i$  from its posterior distribution,  $P(\Theta_i|Y, M_i)$ , are made for the purpose of statistical inference. Hence no additional sample is needed for implementing the bridge sampling.

Our key aim here is to improve the efficiency of bridge sampling estimators when the underlying densities are multi-modal, as is common for complex models. Section 2 briefly overviews warp bridge sampling (Meng and Schilling, 2002), highlighting its power in increasing distribution overlaps. Section 3 introduces a class of stochastic transformations, Warp-U transformations, that can warp two multi-modal densities into having substantial overlap without altering their normalizing constants. Section 4 outlines a computationally efficient strategy for finding a specific transformation and studies the properties of the corresponding estimator, and Section 5 compares both the computational cost and the statistical efficiency of estimators with different tuning parameters, aiming to provide practical guidance for choosing them. Section 6 explores a different direction of using Warp-U transformations for the purpose of improving MCMC algorithms, especially for sampling from multi-modal distributions.

## 2 Literature Review: Warp Bridge Sampling

Bridge sampling (Bennett, 1976; Meng and Wong, 1996) estimates the ratio of the normalizing constants of two unnormalized densities by leveraging the overlap between the two densities. Therefore, any method that can increase this overlap has the potential of reducing the MC error. The warp bridge sampling of Meng and Schilling (2002) explored this idea by transforming the simulated data so that the densities of the transformed data have substantially more overlap.

To fix the idea, for  $i = 1, 2$ , let  $q_i$  be the two unnormalized densities with respect to a common measure  $\mathbf{u}$ , each with a normalizing constant  $c_i$ . We use  $p_i$  to denote the normalized density, i.e.,  $p_i(\omega) = c_i^{-1}q_i(\omega)$ , for  $\omega \in \Omega_i$ , where  $\Omega_i$  is the support of  $q_i$ . We are interested in estimating the ratio  $r = c_1/c_2$  or  $\lambda = \log(r)$ , using the *given* draws,  $\{w_{i,1}, w_{i,2}, \dots, w_{i,n_i}\}$ , from  $p_i$ ,  $i = 1, 2$ .

### 2.1 Bridge Sampling

Bridge sampling relies on a simple fact that for any function,  $\alpha$ , defined on  $\Omega_1 \cap \Omega_2$  and satisfying  $0 < \left| \int_{\Omega_1 \cap \Omega_2} \alpha(\omega) p_1(\omega) p_2(\omega) \mathbf{u}(d\omega) \right| < \infty$ , the following identity holds;

$$r = \frac{c_1}{c_2} = \frac{\mathbb{E}_2[q_1(\omega)\alpha(\omega)]}{\mathbb{E}_1[q_2(\omega)\alpha(\omega)]}, \quad (1)$$

where  $\mathbb{E}_i$  represents the expectation with respect to  $p_i$ . The corresponding bridge sampling estimator of  $r$  is then the sample counterpart of (1), i.e.,

$$\hat{r}_\alpha = \frac{n_2^{-1} \sum_{j=1}^{n_2} q_1(w_{2,j}) \alpha(w_{2,j})}{n_1^{-1} \sum_{j=1}^{n_1} q_2(w_{1,j}) \alpha(w_{1,j})}. \quad (2)$$

Different choices of  $\alpha$  lead to estimators with different statistical efficiencies, quantified by the asymptotic variance of  $\hat{\lambda}_\alpha = \log(\hat{r}_\alpha)$ , or equivalently, the asymptotic relative variance of  $\hat{r}_\alpha$ ,  $\mathbb{E}(\hat{r}_\alpha - r)^2/r^2$ . Under the assumption that all the MC draws used in (2) are mutually independent, Meng and Wong (1996) showed that the first-order asymptotic variance of  $\hat{\lambda}_\alpha$  is given by  $(n_1 + n_2)^{-1} \mathcal{V}_\alpha(p_1, p_2)$ , where

$$\mathcal{V}_\alpha(p_1, p_2) = \frac{\int p_1^* p_2^* (p_1^* + p_2^*) \alpha^2 \mathbf{u}(d\omega)}{\left( \int p_1^* p_2^* \alpha \mathbf{u}(d\omega) \right)^2} - \frac{1}{s_1} - \frac{1}{s_2}, \quad (3)$$

with  $s_i = n_i/(n_1 + n_2)$  and  $p_i^* = s_i p_i$ .

Both the importance sampling and the geometric bridge sampling are special cases of bridge sampling, with  $\alpha_{\text{imp}} \propto 1/q_2$  and  $\alpha_{\text{geo}} \propto 1/\sqrt{q_1 q_2}$ , respectively. Meng and Wong (1996) showed that the asymptotic relative variance of the geometric bridge sampling estimator,  $\hat{r}_{\text{geo}}$ , is

$$\text{Var} \left( \hat{\lambda}_{\text{geo}} \right) = \left( \frac{1}{n_1} + \frac{1}{n_2} \right) \left\{ b \left[ 1 - H_{\mathbb{E}}^2(p_1, p_2) \right]^{-2} - 1 \right\} + o \left( \frac{1}{n_1 + n_2} \right), \quad (4)$$

where  $\hat{\lambda}_{\text{geo}} = \log(\hat{r}_{\text{geo}})$ ,  $b = \int_{\Omega_1 \cap \Omega_2} [p_1^*(\omega) + p_2^*(\omega)] \mathbf{u}(\mathrm{d}\omega) \leq 1$ , and  $H_{\text{E}}(p_1, p_2)$  is the Hellinger distance between  $p_1$  and  $p_2$ , defined as

$$H_{\text{E}}(p_1, p_2) = \left[ \frac{1}{2} \int \left( \sqrt{p_1(\omega)} - \sqrt{p_2(\omega)} \right)^2 \mathbf{u}(\mathrm{d}\omega) \right]^{1/2}. \quad (5)$$

When all the draws are independent, Meng and Wong (1996) found that the optimal choice of  $\alpha$  in terms of minimizing the asymptotic variance of  $\hat{\lambda}_{\alpha}$  is

$$\alpha_{\text{opt}}(\omega) \propto \frac{1}{s_1 q_1(\omega) + r s_2 q_2(\omega)}.$$

Because  $\alpha_{\text{opt}}$  depends on the unknown quantity  $r$ , Meng and Wong (1996) proposed an iterative sequence that converges to the optimal bridge sampling estimator,  $\hat{r}_{\text{opt}}$ , i.e.,

$$\hat{r}_{\text{opt}}^{(t+1)} = \frac{\frac{1}{n_2} \sum_{j=1}^{n_2} \left[ \frac{l_{2,j}}{s_1 l_{2,j} + s_2 \hat{r}_{\text{opt}}^{(t)}} \right]}{\frac{1}{n_1} \sum_{j=1}^{n_1} \left[ \frac{1}{s_1 l_{1,j} + s_2 \hat{r}_{\text{opt}}^{(t)}} \right]}, \quad (6)$$

where  $l_{i,j} = q_1(w_{i,j})/q_2(w_{i,j})$ , for  $i = 1, 2$ , and  $j = 1, 2, \dots, n_i$ . The sequence typically converges to  $\hat{r}_{\text{opt}}$  within a few iterations (e.g., 10) in many applications. Meng and Wong (1996) showed that the asymptotic variance of  $\hat{\lambda}_{\text{opt}} = \log(\hat{r}_{\text{opt}})$  is the same as that of the un-realizable  $\log(\hat{r}_{\alpha_{\text{opt}}})$ , that is, there is no loss of efficiency (asymptotically) due to adaptation via iteration (6). Specifically,

$$\text{Var}(\hat{\lambda}_{\text{opt}}) = \left( \frac{1}{n_1} + \frac{1}{n_2} \right) \left[ (1 - H_{\text{A}}(p_1, p_2))^{-1} - 1 \right] + o\left( \frac{1}{n_1 + n_2} \right), \quad (7)$$

where  $H_{\text{A}}(p_1, p_2)$  is the (sample-size adjusted) harmonic divergence between  $p_1$  and  $p_2$  given by

$$H_{\text{A}}(p_1, p_2) = 1 - \int_{\Omega_1 \cap \Omega_2} [w_1 p_1^{-1}(\omega) + w_2 p_2^{-1}(\omega)]^{-1} \mathbf{u}(\mathrm{d}\omega), \quad (8)$$

where  $w_i = s_i^{-1}/(s_1^{-1} + s_2^{-1})$ ,  $i = 1, 2$ . Via a likelihood that treats the baseline measure  $\mathbf{u}$  as the (infinite dimensional) parameter, Kong et al. (2003) showed that  $\hat{r}_{\text{opt}}$  is an MLE, and hence further confirms its optimality.

## 2.2 Warp Bridge Sampling

From (4) and (7), we see that if we apply transformation  $\mathcal{F}_i$ , to  $w_{i,j}$  such that (A) the unnormalized density,  $\tilde{q}_i$ , of the transformed data,  $\tilde{w}_{i,j} = \mathcal{F}_i(w_{i,j})$ , has the same normalizing constant as  $q_i$ , and (B)  $H_{\text{E}}(\tilde{p}_1, \tilde{p}_2) < H_{\text{E}}(p_1, p_2)$  and/or  $H_{\text{A}}(\tilde{p}_1, \tilde{p}_2) < H_{\text{A}}(p_1, p_2)$ , then the corresponding bridge sampling estimator (e.g., geometric and/or optimal) based on  $\{(\tilde{w}_{i,1}, \dots, \tilde{w}_{i,n_i}); i = 1, 2\}$  will have smaller asymptotic variance than that based on  $\{(w_{i,1}, \dots, w_{i,n_i}); i = 1, 2\}$ . Warp transformations (Meng and Schilling, 2002) were motivated exactly by this observation.

In particular, Warp-I transformation moves one density closer to another to increase their overlap. Let  $\mu$  be a location parameter, e.g., the difference between the means or between the

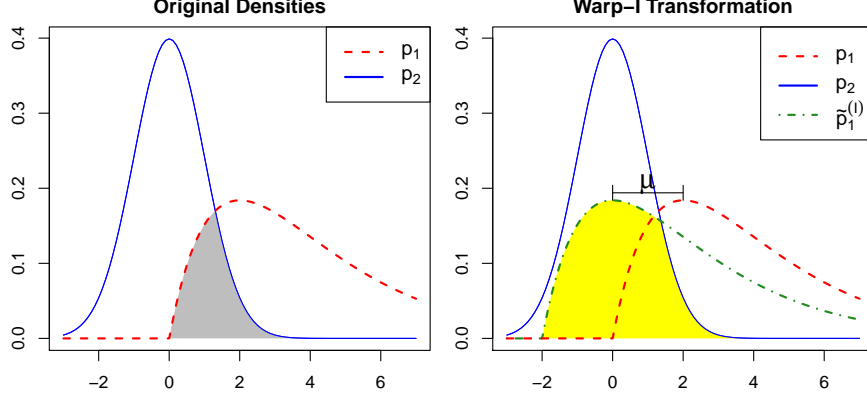


Figure 1: Graphical illustration of Warp-I transformation. The dashed and the solid lines are the curves of  $p_1$  and  $p_2$ . The dash-dot line is the density,  $\tilde{p}_1^{(I)}$ , of the Warp-I transformed data, obtained by moving  $p_1$  to the left by  $\mu$  units. The shaded areas are the overlap between two densities.

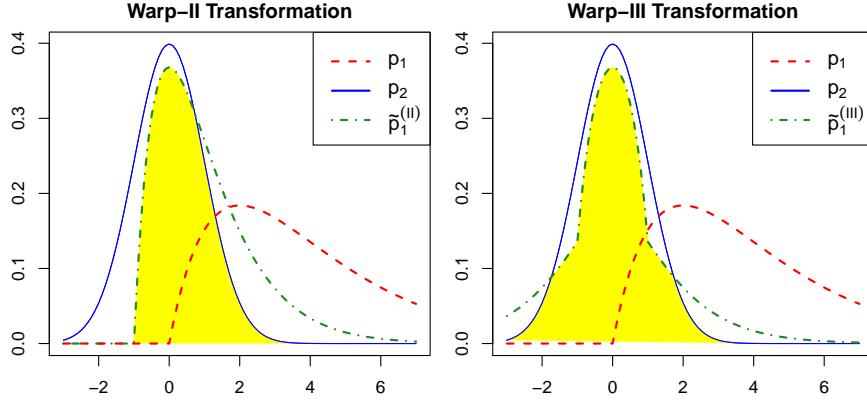


Figure 2: Graphical illustration of Warp-II (left) and Warp-III transformations (right). The dashed and the solid lines are the curves of  $p_1$  and  $p_2$ . The dash-dot lines are  $p_1^{(II)}$  (left) and  $p_1^{(III)}$  (right), obtained by Warp-II and Warp-III transformation, respectively.

modes of the two densities. We then let  $\tilde{w}_{1,j}^{(I)} = w_{1,j} - \mu$  and  $\tilde{w}_{2,j}^{(I)} = w_{2,j}$ , and accordingly we have  $\tilde{q}_1^{(I)}(w) = q_1(w + \mu)$  and  $\tilde{q}_2^{(I)} = q_2$ , respectively. The Warp-I bridge sampling estimator is then obtained by replacing  $w_{i,j}$  and  $q_i$  in (2) with  $\tilde{w}_{i,j}^{(I)}$  and  $\tilde{q}_i^{(I)}$ , respectively. Figure 1 shows the densities before (left panel) and after (right panel) Warp-I transformation, demonstrating the substantially increased overlap.

The next level transformation is to match both the center and the spread. Let  $\mu_i$  be a location parameter and  $\mathcal{S}_i$  be a scaling parameter. The Warp-II transformation is then  $\tilde{w}_{i,j}^{(II)} = \mathcal{S}_i^{-1}(w_{i,j} - \mu_i)$ , the unnormalized density of which is  $\tilde{q}_i^{(II)}(\omega) = |\mathcal{S}_i|q_i(\mathcal{S}_i\omega + \mu_i)$ . The dash-dot curve in Figure 2 (left) is an example of  $\tilde{p}_1^{(II)}$ , which has more overlap with  $p_2$  than  $p_1$  or  $\tilde{p}_1^{(I)}$  has.

The third order consideration (in terms of the order of moments) naturally would be symmetry, which can be done nicely via a *stochastic transformation*. Specifically, a Warp-III transformation sets  $w_{i,j} = \xi_j \mathcal{S}_i^{-1}(w_{i,j} - \mu_i)$ , where  $\xi_j$  takes on value 1 or  $-1$  with equal probability (independently of  $w_{i,j}$ ) to induce symmetry. Its unnormalized density is  $\tilde{q}_i^{(\text{III})}(\omega) = |\mathcal{S}_i| [q_i(\mu_i - \mathcal{S}_i\omega) + q_i(\mu_i + \mathcal{S}_i\omega)]/2$ , an example of which is shown in Figure 2 (right; the dash-dot curve). Below we show that the idea of stochastic transformations is also very powerful in dealing multi-modality, a thorny issue in MC (and in statistical inference in general).

### 3 Warp-U Bridge Sampling

We begin by focusing on estimating a single normalizing constant and fix the other density to be a common density,  $\phi$ , such as  $\mathcal{N}(0, I_d)$  or  $t$ -distribution. This makes it easier to see the essence of our method, i.e., to transform the data so that the corresponding density will be close to  $\phi$ . The problem of estimating a ratio of two normalizing constants can then be handled by either (i) two bridge sampling estimators for the numerator and denominator of the ratio separately based on the transformed dataset  $\{\tilde{w}_{i,1}, \dots, \tilde{w}_{i,n_i}\} \stackrel{iid}{\sim} \tilde{p}_i$  and  $\{z_{i,1}, \dots, z_{i,m_i}\} \stackrel{iid}{\sim} \phi$ , for  $i = 1, 2$  (and the draws from  $\phi$  can be shared), or (ii) one bridge sampling estimator of the ratio directly based on the two transformed datasets  $\{\tilde{w}_{i,1}, \dots, \tilde{w}_{i,n_i}\} \stackrel{iid}{\sim} \tilde{p}_i$  for  $i = 1, 2$ . Strategy (ii) is effective because two densities tend to overlap substantially when they both overlap significantly with a common density (see Section 5.5).

Since we focus on a single  $q$ , we drop the double indices and let  $\{w_1, \dots, w_n\}$  be  $n$  i.i.d draws from  $p = c^{-1}q$ , where  $p$  is assumed to be a continuous density in  $R^d$ . We denote  $\{z_1, \dots, z_m\}$  to be i.i.d draws from a chosen density  $\phi$ . For concreteness, we will fix  $\phi$  to be  $\mathcal{N}(0, I_d)$  throughout the paper, but many other choices of  $\phi$  can work equally well or even better.

#### 3.1 Definition and Intuition of Warp-U Transformation

At the center of the proposed Warp-U transformation is a Gaussian mixture distribution, i.e.,

$$\phi_{\text{mix}}(\omega; \zeta) = \sum_{k=1}^K \phi^{(k)}(\omega) = \sum_{k=1}^K \pi_k |\mathcal{S}_k|^{-1} \phi(\mathcal{S}_k^{-1}(\omega - \mu_k)), \quad (9)$$

where  $\phi$  is the pdf of  $\mathcal{N}(0, I)$ ,  $\phi^{(k)}$  represents the  $k$ -th component in  $\phi_{\text{mix}}$ , including its weight  $\pi_k$ , for  $k = 1, \dots, K$ , and  $\zeta$  collects the transformation parameters  $\{(\pi_k, \mu_k, \mathcal{S}_k) : k = 1, \dots, K\}$ . Alspach and Sorenson (1972) showed that a Gaussian sum approximation in the form of (9) can converge uniformly to any piecewise continuous density function. So for a reasonable choice of  $K$ , we should be able to find a  $\phi_{\text{mix}}$  that has sufficient overlap with  $p$ . Section 4 will discuss how to estimate  $\phi_{\text{mix}}$ . Here we assume  $\phi_{\text{mix}}$  is known, to first describe the Warp-U transformation.

Specifically, the left plot of Figure 3 displays an example of  $p$  (dashed line) and  $\phi_{\text{mix}}$  (solid line) with reasonable overlap. We then apply a *stochastic transformation*, which will be illustrated

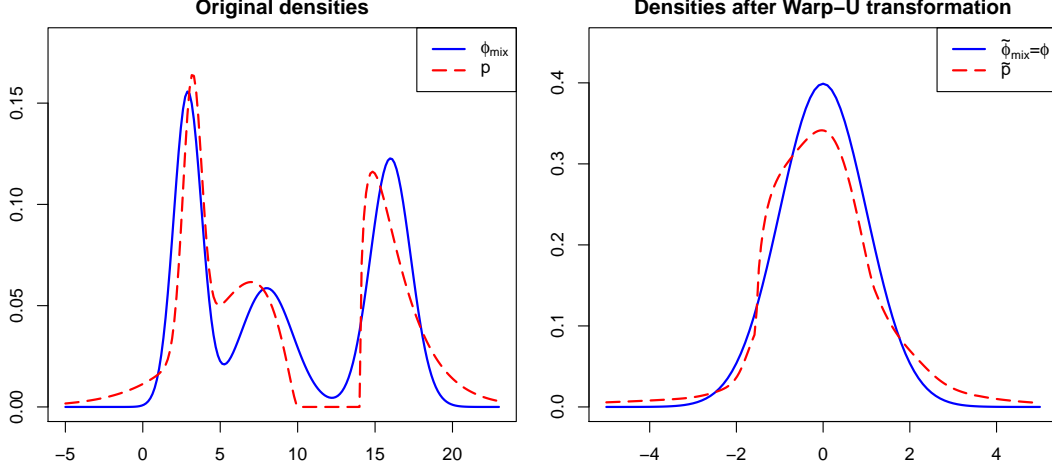


Figure 3: (Left) density  $p$  (dashed line) and a Gaussian mixture density  $\phi_{\text{mix}}$  (solid line), which has substantial overlap with  $p$ ; (Right) after Warp-U transformation,  $\phi_{\text{mix}}$  turns into the standard normal distribution (solid line) and  $p$  turns into  $\tilde{p}^{(U)}$  (dashed line).

in Figure 4, to both of them to produce  $\tilde{p}$  (dashed line) and  $\phi$  (solid line), as in the right plot of Figure 3, respectively. The solid curve on the vertical plate in Figure 4(a) is  $\phi_{\text{mix}}$ , which is decomposed into three components,  $\phi^{(k)}$ , for  $k = 1, 2, 3$ , corresponding to the three solid curves in Figure 4(b). Each component,  $\phi^{(k)}$ , is moved by  $\mu_k$  units to the origin and then rescaled by  $\mathcal{S}_k^{-1}$ , resulting in  $\pi_k \phi$ , as shown in Figure 4(d) (the solid curves). So after the transformation, the sum of the three components becomes  $\phi$ .

From another prospective, if  $X \sim \phi_{\text{mix}}$ , then  $X$  can be represented stochastically as  $X = \mathcal{S}_\Theta Z + \mu_\Theta$ , where  $Z \sim \phi$ ,  $\Theta$  is a discrete random variable with a probability mass function  $P(\Theta = k) = \pi_k$  for  $k = 1, 2, 3$ , and  $\Theta$  and  $Z$  are independent. Figure 4(b) shows the joint distribution of  $\Theta$  and  $X$ , with their marginal distributions on the two vertical plates. The random index  $\Theta$  induces a random transformation (e.g., it is a random variable for given  $x$ )

$$\mathcal{F}_\Theta(x; \zeta) = \mathcal{S}_\Theta^{-1}(x - \mu_\Theta). \quad (10)$$

By applying  $\mathcal{F}_\Theta$  to  $X$ , we obtain  $\mathcal{F}_\Theta(X; \zeta) = Z$ , and thus turning  $\phi_{\text{mix}}$  into  $\phi$ . So if  $(x_i, \theta_i)$  is drawn from the joint distribution of  $(X, \Theta)$ , then  $\tilde{x}_i = \mathcal{S}_{\theta_i}^{-1}(x_i - \mu_{\theta_i})$  is a draw from  $\phi$ .

Now we describe how to wrap  $p$  into  $\tilde{p}$ , the dashed line in Figure 3. Let  $W$  be a random variable from  $p$ . We then construct a random index  $\Psi$  whose conditional distribution given  $W = w$  is the same as the conditional distribution of  $\Theta$  given  $X = w$ . That is,

$$\varpi(k|\omega) \triangleq P(\Psi = k|W = \omega) \equiv P(\Theta = k|X = \omega) = \phi^{(k)}(\omega)/\phi_{\text{mix}}(\omega), \quad k = 1, \dots, K. \quad (11)$$

As a result,  $p$  is also decomposed into  $K$  components, i.e.,  $p(\omega) = \sum_{k=1}^K p^{(k)}(\omega)$ , where

$$p^{(k)}(\omega) = p(\omega, \Psi = k) = p(\omega) \frac{\phi^{(k)}(\omega)}{\phi_{\text{mix}}(\omega)}. \quad (12)$$

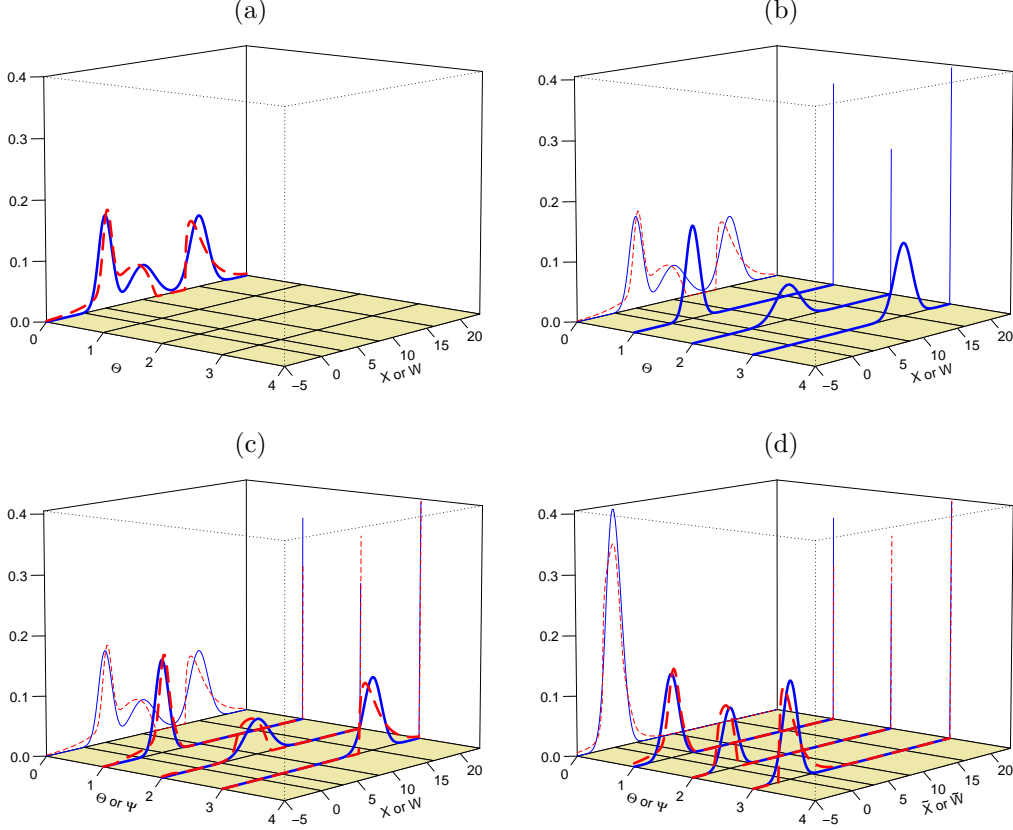


Figure 4: Illustration of Warp-U transformation. (a)  $\phi_{\text{mix}}$  (solid line) and  $p$  (dashed line); (b) the joint and marginal distributions of  $X$  and  $\Theta$  (solid line); (c) the joint and marginal distributions of  $W$  and  $\Psi$  (dashed line); (d) the joint and marginal distributions of  $\Theta$  and  $\tilde{X}$  (solid line) and those of  $\Psi$  and  $\tilde{W}$  (dashed line), where  $\tilde{X}$  and  $\tilde{W}$  are obtained via Warp-U transformation.

Figure 4(c) shows the joint distribution of  $(W, \Psi)$  (thick dashed curves) and their marginal distributions (thin dash curves in the two vertical plates).

The Warp-U transformation applied to  $W$  is then defined via the same random map in (10):

$$\tilde{W} = \mathcal{F}_{\Psi}(W; \zeta) = \mathcal{S}_{\Psi}^{-1}(W - \mu_{\Psi}) \sim \tilde{p}. \quad (13)$$

To apply a Warp-U transformation to the data  $w_j$ , we first calculate  $\varpi(\cdot|w_j)$  according to (11), then draw  $\psi_j$  from  $\varpi(\cdot|w_j)$ , and finally apply the deterministic transformation  $\mathcal{F}_{\psi_j}$  to  $w_j$ . Graphically, each  $p^{(k)}$  in Figure 4(c) is re-centered and re-scaled, like its counterpart,  $\phi^{(k)}$ . The dashed lines in Figure 4(d) are the joint distribution of  $\Psi$  and the Warp-U transformed variable,  $\tilde{W}$ , the marginal distribution of which has a substantial overlap with  $\phi$ .

We remark that when  $K = 1$ , Warp-U transformation does not produce more overlap beyond the original matching via fitting  $\phi_{\text{mix}}$  to  $p$ , which is the same as Warp-II transformation when we choose  $\phi_{\text{mix}}$  to be a location-scale family. When  $K > 1$ , Theorem 1 in Section 3.2 below ensures



that there will be additional overlap between  $\tilde{p}$  and  $\phi$  compared to the overlap between  $p$  and  $\phi_{\text{mix}}$ , unless  $p = \phi_{\text{mix}}$  already or the warp transformation is essentially a trivial one.

### 3.2 A Key Theorem for Warp-U Transformation

Figure 5 summarizes all the key variables and distributions underlying a Warp-U transformation, as described above, but the “index variable”  $\Theta$  (and hence also  $\Psi$ ) is permitted to take on an arbitrary distribution  $\pi$  on  $\Pi$  with dominating measure  $\mathbf{v}$ , no longer restricted to be discrete. We assume  $\phi$  is chosen such that it shares the same support of our target  $p$ , denoted by  $\Omega$ , and that the map  $X = \mathcal{H}_\theta(Z)$  is chosen such that for any given value of  $\theta \in \Pi$ ,  $\mathcal{H}_\theta(\cdot)$  is one-to-one, almost surely (with respect to  $\mathbf{u}$ ) differentiable, and  $\Omega = \mathcal{H}_\theta(\Omega)$ . We denote its inverse map by  $Z = \mathcal{F}_\theta(X)$ . The conditional distribution  $X|\Theta = \theta$  is then<sup>1</sup>

$$\phi_{X|\Theta}(\omega|\theta) = \phi(\mathcal{F}_\theta(\omega)) |\mathcal{F}'_\theta(\omega)|, \quad \omega \in \Omega \quad (14)$$

and the (marginal) density of  $X$  is

$$\phi_{\text{mix}}(\omega) = \int_{\Pi} \phi_{X|\Theta}(\omega|\theta) \pi(\theta) \mathbf{u}(\mathrm{d}\theta) = \int_{\Pi} \phi(\mathcal{F}_\theta(\omega)) |\mathcal{F}'_\theta(\omega)| \pi(\theta) \mathbf{u}(\mathrm{d}\theta). \quad (15)$$

Let  $\varpi(\cdot|\omega)$  be the conditional distribution  $\Theta|X = \omega$ ,

$$\varpi(\theta|\omega) = \frac{\phi_{X|\Theta}(\omega|\theta) \pi(\theta)}{\phi_{\text{mix}}(\omega)}, \quad \theta \in \Pi, \quad (16)$$

and, as before, the variable  $\Psi$  be defined through  $P(\Psi = \theta|W = \omega) = \varpi(\theta|\omega)$ . The joint distributions of  $(\Psi, W)$  and  $(\Theta, X)$  therefore share the same conditional specification:

$$p_{\Psi, W}(\theta, \omega) = \varpi(\theta|\omega) p(\omega) \quad \text{and} \quad \phi_{\Theta, X}(\theta, \omega) = \varpi(\theta|\omega) \phi_{\text{mix}}(\omega), \quad (\theta, \omega) \in \Pi \times \Omega. \quad (17)$$

It is this same conditioning, a form of coupling, that creates the overlap between  $\phi$  and the Warp-U transformed  $W : \widetilde{W} = \mathcal{F}_\Psi(W) \sim \tilde{p}$ , beyond that between  $\phi_{\text{mix}}$  and  $p$ .

To prove this mathematically, we will need a measure of overlap. The notion of  $f$ -divergence, or more precisely its complement (since small divergence corresponds to large overlap), serves well as a general class for our purposes. For any (non-trivial) *convex* function  $f$  on  $[0, \infty)$  such that  $f(1) = 0$ , the corresponding  $f$ -divergence between two probability densities  $p_1$  and  $p_2$ , when  $p_1$  is absolutely continuous with respect to  $p_2$ , is defined as

$$\mathcal{D}_f(p_1||p_2) = \int_{\Omega} p_2(\omega) f\left(\frac{p_1(\omega)}{p_2(\omega)}\right) \mathbf{u}(\mathrm{d}\omega). \quad (18)$$

We prove below that any Warp-U transformation will reduce any  $f$ -divergence, unless either the transformation or  $f$  (or both) is trivially chosen, in which cases the  $f$ -divergence is unchanged.

**Theorem 1.** Suppose our warp transformation is defined as in Figure 5, with the conditions given in its caption. The following results then hold.

<sup>1</sup>Note here  $\phi$  is used as a genetic notation, hence it is not necessarily the pdf of  $\mathcal{N}(0, I_d)$ .

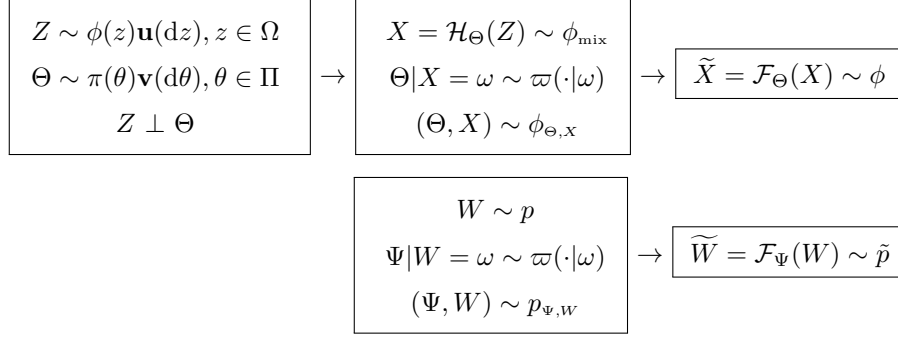


Figure 5: Relationships among the random variables and their distributions for Warp-U transformation. Here we assume that for almost surely (with respect to  $\mathbf{v}$ ) all values of  $\theta \in \Pi$ ,  $\mathcal{F}_\theta$  and its inverse  $\mathcal{H}_\theta$  are one-to-one, onto, and almost surely (with respect to  $\mathbf{u}$ ) differentiable maps from  $\Omega \rightarrow \Omega$ .

(I) For any  $f$ -divergence  $\mathcal{D}_f$ , we have  $\mathcal{D}_f(\tilde{p}|\phi) \leq \mathcal{D}_f(p|\phi_{\text{mix}})$ .

(II) If  $f$  is strict convex, then the equality in (I) holds if and only if  $\ell(\theta; \tilde{\omega}) \equiv \frac{p(\mathcal{H}_\theta(\tilde{\omega}))}{\phi_{\text{mix}}(\mathcal{H}_\theta(\tilde{\omega}))}$  is free of  $\theta$  (almost surely with respect to  $\mathbf{v} \times \mathbf{u}$ ).

*Proof.* Let  $t(\theta, \omega) = \mathcal{F}_\theta(\omega)$ , then we can write  $\tilde{W} = t(\Psi, W)$  and  $\tilde{X} = t(\Theta, X)$ . Therefore,  $\tilde{p}$  and  $\phi$  are determined by  $p_{\Psi, W}$  and  $\phi_{\Theta, X}$  of (17) respectively, via the *same* map  $t : \Pi \times \Omega \rightarrow \Omega$ . Claim (I) then follows from the well-known monotone property of  $f$ -divergence (Ali and Silvey, 1966):

$$\mathcal{D}_f(\tilde{p}|\phi) \leq \mathcal{D}_f(p_{\Psi, W}|\phi_{\Theta, X}) = \mathcal{D}_f(p|\phi_{\text{mix}}), \quad (19)$$

where the last equality holds because  $p_{\Psi, W}/\phi_{\Theta, X} = p/\phi_{\text{mix}}$ , a consequence of (17).

To prove (II), it is known that when  $f$  is strictly convex (Ali and Silvey, 1966), the (first) inequality in (17) becomes an equality if and only if  $t$  is a sufficient statistics for the distribution family  $\{p_{\Psi, W}, \phi_{\Theta, X}\}$ . By the well-known factorization theorem for sufficiency, the latter condition is the same as requiring  $p_{\Psi, W}(\theta, \omega)/\phi_{\Theta, X}(\theta, \omega)$  to depend on  $(\theta, \omega)$  only through  $t = t(\theta, \omega) = \mathcal{F}_\theta(\omega)$ , almost surely with respect to  $\mathbf{v} \times \mathbf{u}$ . But from (17) and  $\omega = \mathcal{F}_\theta^{-1}(t) = \mathcal{H}_\theta(t)$ , we have

$$p_{\Psi, W}(\theta, \omega)/\phi_{\Theta, X}(\theta, \omega) = p(\mathcal{H}_\theta(t))/\phi_{\text{mix}}(\mathcal{H}_\theta(t)) = \ell(\theta; t).$$

Consequently,  $t$  is sufficient if and only if  $\ell(\theta; t)$  is free of  $\theta$ , and hence (II).  $\square$

The Hellinger distance, the weighted harmonic divergency in (8), and the  $L_1$  distance are all examples of  $f$ -divergence, respectively with  $f_{H_e}(t) = 0.5(1 - \sqrt{t})^2$ ,  $f_{H_a}(t) = w_1(1 - t)/(w_1 + w_2t)$ , and  $f_{L_1}(t) = |1 - t|$ . However, the inequality (I) does not necessarily hold for  $L_p$  distance when  $p \neq 1$  (and hence  $L_p$  distance is not an  $f$ -divergence when  $p \neq 1$ ). As a simple counterexample, let  $K = 1$  in (9) and therefore  $\phi_{\text{mix}}(\omega) = |\mathcal{S}|^{-1}\phi(\mathcal{S}^{-1}(\omega - \mu))$ . Then  $\tilde{p}(\omega) = |\mathcal{S}|p(\mathcal{S}\omega + \mu)$ , and

$$L_p(\tilde{p}, \phi) = \left( \int \|\mathcal{S}|p(\mathcal{S}\tilde{\omega} + \mu) - \phi(\tilde{\omega})|^p \mathbf{u}(d\tilde{\omega}) \right)^{1/p} = |\mathcal{S}|^{1-1/p} L_p(p, \phi_{\text{mix}}),$$

so  $L_p(\tilde{p}, \phi) > L_p(p, \phi_{\text{mix}})$  whenever  $|\mathcal{S}|^{1-1/p} > 1$  (and  $L_p(p, \phi_{\text{mix}}) > 0$ ).

We also remark that the condition (II) means that a warp transformation will always result in real gain, as measured by any strictly convex  $f$ -divergence, unless (A)  $\phi_{\text{mix}}$  is already a perfect fit to  $p$ , in which case obviously  $\ell(\theta, \tilde{\omega}) = 1$ ; or (B)  $p \neq \phi_{\text{mix}}$ , but the warp transformation  $\mathcal{F}_\Theta$  is unfortunately (or unwisely) chosen that it renders the “likelihood ratio”  $\ell(\theta; \tilde{\omega})$  flat as a function of  $\theta$ . Situation (B) includes the obvious case where  $\mathcal{F}_\theta$  does not actually depend on  $\theta$ , or  $\theta$  does not vary because  $\pi$  is a singleton. For a seemingly non-obvious case of (B), suppose our  $p(\omega)$  happens to be a “length-biased” version of a mixture of  $\phi(\omega)$  and its “mirror reflection”<sup>2</sup>  $\phi(-\omega)$ , i.e.,  $p(\omega) = |\omega|[\alpha\phi(\omega) + (1-\alpha)\phi(-\omega)]/c$ , where  $0 < \alpha < 1$ , and  $c = \mathbb{E}_\phi(|Z|)$  is nonzero and finite. Noticing this “mirror mixing” nature, we may naturally consider  $\mathcal{F}_\Theta(\omega) = \Theta\omega$ , where  $\Theta = 1$  and  $-1$  with probability  $\beta$  and  $1 - \beta$  respectively (when  $\beta = 1/2$ , it reduces to the Warp-III transformation illustrated in Section 2.2). This would lead to  $\phi_{\text{mix}}(\omega) = \beta\phi(\omega) + (1 - \beta)\phi(-\omega)$ . Suppose, by an unfortunate coincidence, the  $\beta$  we choose happens to be exactly the same as  $\alpha$ . Consequently  $p(\omega) = |\omega|\phi_{\text{mix}}(\omega)/c$ , yielding  $\ell(\theta; \tilde{\omega}) = |\theta\tilde{\omega}|/c = |\tilde{\omega}|/c$ , and hence it is free of  $\theta$ .

Intuitively, the mirror reflection does nothing to the “length bias” correction because the length is invariant to the sign of the variable  $Z$ , so if our warp transformation has rendered the exact match between the pre-correction version of  $p$  and the mixture  $\phi_{\text{mix}}$ , then further Warp-U matching will have no effect on increasing the overlap. The next section graphically illustrates where the further gains come from, which would make it clearer why in this contrived example the further gain is zero. We label this example as “contrived”, because in practice for (A) or (B) to occur it would require far more knowledge (or extreme luck!) than we have for finding a computationally convenient approximation  $\phi_{\text{mix}}$  to  $p$  unless, of course, we make some mindless choices of our warp transformations, such as a mirror reflection when  $p$  is already symmetric.

### 3.3 Graphical Illustration of Theorem 1

The transformation given in Section 3.1 is a special case of a Warp-U transformation, where  $\Theta$  is a discrete random variable with  $P(\Theta = k) = \pi_k$ , and  $\mathcal{H}_k(\tilde{\omega}) = \mathcal{S}_k\tilde{\omega} + \mu_k$ . This case illustrates well how a Warp-U transformation increases the overlapping area between  $p_1$  and  $p_2$ :

$$O(p_1, p_2) = \int \min\{p_1, p_2\} \mathbf{u}(d\omega) = \int p_1 \min\left\{1, \frac{p_2}{p_1}\right\} \mathbf{u}(d\omega) = 1 - L_1(p_1, p_2)/2.$$

Hence a decrease of  $L_1$  distance necessarily increases the overlap.

Figure 6(a) shows a tri-modal distribution  $p$  (dashed curve) and  $\phi_{\text{mix}}$  with  $K = 2$  components (solid line). The decomposition of  $p$  is determined by  $\phi_{\text{mix}}$ , i.e.,  $p^{(k)} = \phi^{(k)}p/\phi_{\text{mix}}$ , because of (17). Figure 6(b) shows  $p^{(1)}$  (thin dashed line) and  $\phi^{(1)}$  (thin solid line), as well as their overlapping region (shaded in red), and Figure 6(c) shows  $p^{(2)}$ ,  $\phi^{(2)}$ , and their overlap (shaded in yellow).

<sup>2</sup>Again, here  $\phi$  is a generic notation, and hence it is not necessarily a symmetric function.

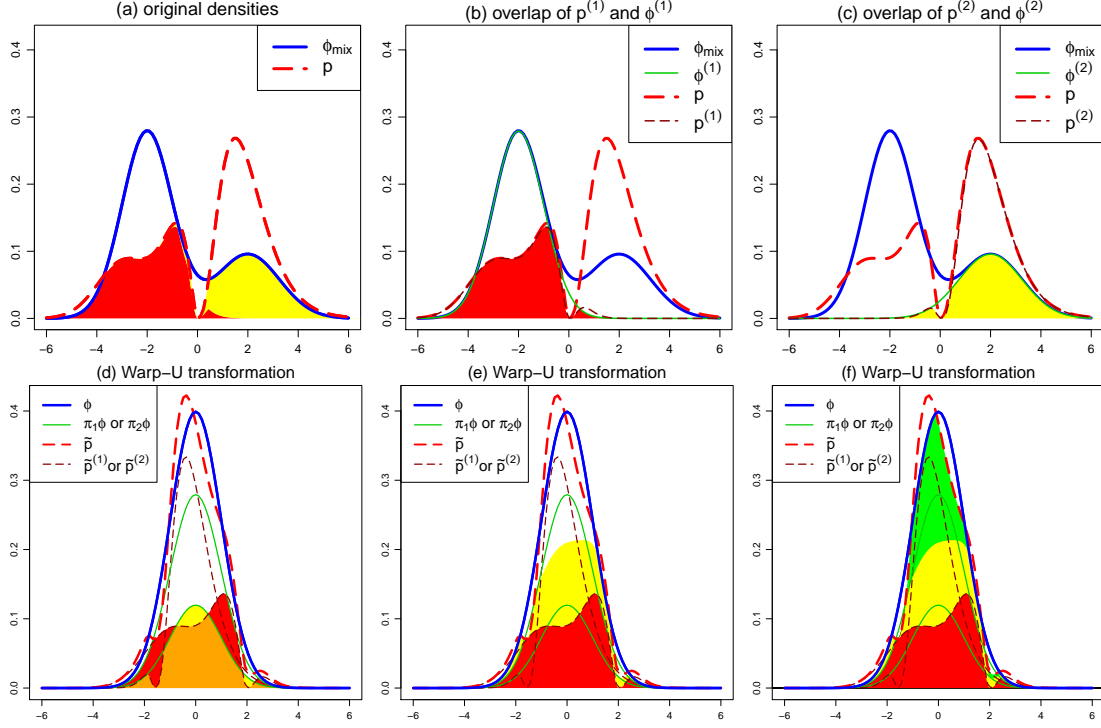


Figure 6: Illustrating the increase in the area of the overlapping region after Warp-U transformation. (a)  $p$  (dashed line) and  $\phi_{\text{mix}}$  (solid line); (b) the 1st component of  $p$ , denoted as  $p^{(1)}$  (thin dashed line), the 1st component of  $\phi_{\text{mix}}$ , denoted as  $\phi^{(1)}$  (thin solid line), and their overlap (shaded in red); (c)  $p^{(2)}$ ,  $\phi^{(2)}$ , and their overlap (shaded in yellow); (d) the corresponding curves and shaded areas after Warp-U transformation; (e) the yellow region is added on top of the red region; (f) the green area shows the additional cross overlap between the 1st and 2nd components induced by the Warp-U transformation.

The overlap of  $p$  and  $\phi_{\text{mix}}$  (shaded region in Figure 6(a)) is exactly the sum of  $O(p^{(k)}, \phi^{(k)})$ , for  $k = 1, \dots, K$ . This is because, for any  $f(x)$ , and hence certainly for  $f(x) = \min\{1, x\}$ , we have

$$\phi_{\text{mix}} f\left(\frac{p}{\phi_{\text{mix}}}\right) = \sum_{k=1}^K \phi^{(k)} f\left(\frac{p^{(k)}}{\phi^{(k)}}\right), \quad (20)$$

which follows from  $\phi_{\text{mix}} = \sum_{k=1}^K \phi^{(k)}$ , and  $p/\phi_{\text{mix}} = p^{(k)}/\phi^{(k)}$  for all  $k$ .

For each  $k$ , a Warp-U transformation leads to the same relocating and rescaling of  $\phi^{(k)}$  and  $p^{(k)}$ . Figure 6(d) shows the resulting  $\tilde{p}^{(k)}$  (thin dashed lines),  $\tilde{\phi}^{(k)}$  (thin solid lines), and their overlapping regions (shaded in red and yellow), which remain the same as those in Figure 6(a) because this is a special case of (B) discussed previously with  $\pi$  being a singleton at  $\Theta = k$ .

Figure 6(e) combines the two shaded regions, which constitute only part of the total overlap of  $\phi$  and  $\tilde{p}$ . The additional overlap, shaded in green in Figure 6(f), is due to the *cross overlap* between  $\tilde{p}^{(k)}$  and  $\tilde{\phi}^{(l)}$ , for any  $l \neq k$ , that is not already included in the overlap between  $\tilde{p}^{(l)}$  and  $\tilde{\phi}^{(l)}$ . Table 1 displays the overlap, the  $L_1$  distance, the Hellinger distance, and the harmonic

Table 1: The area of the overlapping region, the  $L_1$  distance, the Hellinger distance, and the harmonic divergence between  $p$  and  $\phi_{\text{mix}}$  and those between  $\tilde{p}$  and  $\phi$ .

densities	Overlap	$L_1$ distance	Hellinger distance	harmonic divergence
$(p, \phi_{\text{mix}})$	0.66	0.68	0.28	0.145
$(\tilde{p}, \phi)$	0.92	0.16	0.08	0.013

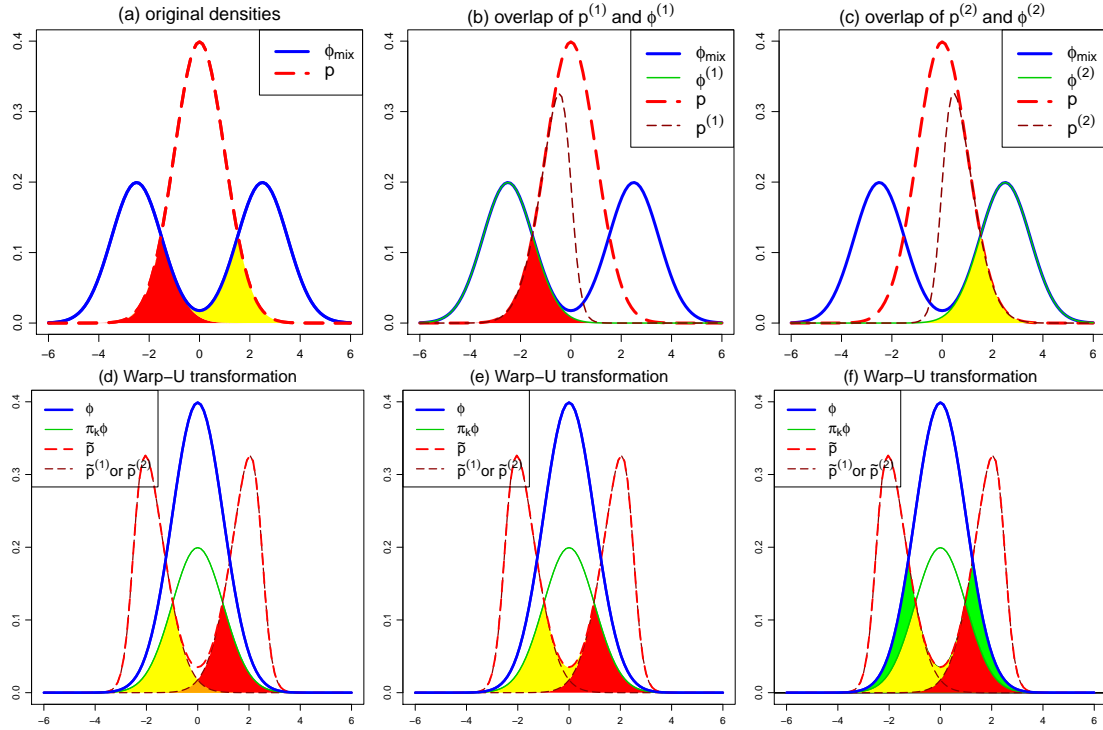


Figure 7: Graphical illustration of the increase of the overlap due to a Warp-U transformation, even as the components  $p^{(1)}$  and  $p^{(2)}$  are moved farther apart. See Figure 6 for more explanation.

divergence between  $p$  and  $\phi_{\text{mix}}$  and those between  $\tilde{p}$  and  $\phi$ . Consistent with Figure 6 and Theorem 1, the overlap increases and all three choices of  $f$ -divergencies decrease after a Warp-U transformation, and rather substantially.

In the example of Figure 6, due to a Warp-U transformation, the two components of  $p$  are scaled and then moved to the origin, and the resulting density  $\tilde{p}$  is a single-modal distribution with more overlap with  $\phi$  than that between  $p$  and  $\phi_{\text{mix}}$ . Figure 7 illustrates that, even if  $\phi_{\text{mix}}$  does not match well with  $p$  and the corresponding Warp-U transformation moves the components  $p^{(k)}$  farther apart,  $O(\phi, \tilde{p}) \geq O(\phi_{\text{mix}}, p)$  still holds. Figure 7(a) shows the uni-modal density  $p$  (dashed line) and the bi-modal density  $\phi_{\text{mix}}$  (solid line), which matches poorly with  $p$ . Figure 7(b,c) highlights  $p^{(1)}$  and  $p^{(2)}$  (thin dashed lines). A Warp-U transformation moves them farther

apart, but it still brings about additional overlap, highlighted in green in Figure 7(f) due to the “cross overlap” between  $\tilde{p}^{(k)}$  and  $\phi^{(l)}$  for  $k \neq l$ .

### 3.4 Warp-U Bridge Sampling

After the Warp-U transformation that is determined by a fixed vector of parameters  $\zeta$  in  $\phi_{\text{mix}}$ , the unnormalized density of the transformed data  $\{\tilde{w}_1, \dots, \tilde{w}_n\}$  can be expressed as

$$\tilde{q}(\omega; \zeta) = \phi(\omega) \sum_{k=1}^K \frac{q(\mathcal{S}_k \omega + \mu_k)}{\phi_{\text{mix}}(\mathcal{S}_k \omega + \mu_k)} \pi_k. \quad (21)$$

Clearly, the normalizing constants of  $\tilde{q}$  and  $q$  are both  $c$ , so we can estimate  $c$  with the bridge sampling estimator based on  $\{\tilde{w}_1, \dots, \tilde{w}_n\} \stackrel{\text{iid}}{\sim} \tilde{p}$  and  $\{z_1, \dots, z_m\} \stackrel{\text{iid}}{\sim} \phi$ , i.e.,

$$\hat{c}_\alpha^{(U)} \equiv \hat{r}_\alpha^{(U)} = \frac{m^{-1} \sum_{j=1}^m \tilde{q}(z_j; \zeta) \alpha(z_j; \tilde{p}, \phi)}{n^{-1} \sum_{j=1}^n \phi(\tilde{w}_j) \alpha(\tilde{w}_j; \tilde{p}, \phi)}. \quad (22)$$

We emphasize that  $\alpha$  is typically a functional of the two densities, e.g., the optimal choice of  $\alpha(\cdot; \tilde{p}, \phi)$  is proportional to  $(s_1 \tilde{p} + s_2 \phi)^{-1}$ . Since  $\phi_{\text{mix}}$  also has some overlap with  $p$ , the normalizing constant can also be estimated with the bridge sampling estimator based on  $\{w_1, \dots, w_n\} \stackrel{\text{iid}}{\sim} p$  and  $\{x_1, \dots, x_m\} \stackrel{\text{iid}}{\sim} \phi_{\text{mix}}$ , i.e.,

$$\hat{c}_\alpha^{(\text{mix})} \equiv \hat{r}_\alpha^{(\text{mix})} = \frac{m^{-1} \sum_{j=1}^m q(x_j) \alpha(x_j; p, \phi_{\text{mix}})}{n^{-1} \sum_{j=1}^n \phi_{\text{mix}}(w_j; \zeta) \alpha(w_j; p, \phi_{\text{mix}})}. \quad (23)$$

Theorem 1 implies  $\mathcal{D}(\tilde{p}, \phi) \leq \mathcal{D}(p, \phi_{\text{mix}})$  for both the harmonic divergence and the Hellinger distance, so the asymptotic variance of  $\hat{\lambda}_\alpha^{(U)} = \log(\hat{c}_\alpha^{(U)})$  is smaller than that of  $\hat{\lambda}_\alpha^{(\text{mix})} = \log(\hat{c}_\alpha^{(\text{mix})})$  for both the geometric and the optimal bridge sampling.

We use simulation to demonstrate the potential of a Warp-U transformation by comparing it with other warp transformations. In this section,  $\phi_{\text{mix}}$  is fixed and  $\zeta$  is independent of  $\{w_1, \dots, w_n\}$ . For example, for fixed  $K$ , we can get  $\zeta$  based on the expression of  $q$ , using methods such as iterative Laplace (Bornkamp, 2011) or fitting a Laplace approximation to each mode (Gelman et al., 2013, Chapter 12). The performance of Warp-U bridge sampling where  $\zeta$  is estimated from draws from  $p$  is explored in Section 4.

The dashed curve in Figure 8(a) is a tri-modal density  $q$ , the normalizing constant of which is to be estimated with  $n = 10^3$  i.i.d draws from it. An additional  $m = 10^3$  i.i.d draws are made from  $\mathcal{N}(0, 1)$  to conduct bridge sampling. As shown in Figure 8(a), the two densities have very little overlap, and the harmonic divergence is 0.865. We apply the optimal bridge sampling algorithm in (6) to the  $N = 10^4$  simulated replicate datasets, and obtain  $N$  vanilla optimal bridge sampling estimates of  $c$  with no transformation, denoted as  $\hat{c}_{\text{opt}}$ . Figure 9(a) shows the histogram of  $\hat{\lambda}_{\text{opt}} - \lambda$ , where  $\hat{\lambda}_{\text{opt}} = \log(\hat{c}_{\text{opt}})$ , which has a root mean square error (RMSE) 0.109.

Figure 8(b) shows that after a Warp-I transformation, the overlap between the two densities increases and their harmonic divergence reduces to 0.528. The histogram of  $\hat{\lambda}_{\text{opt}}^{(I)} - \lambda$  is shown

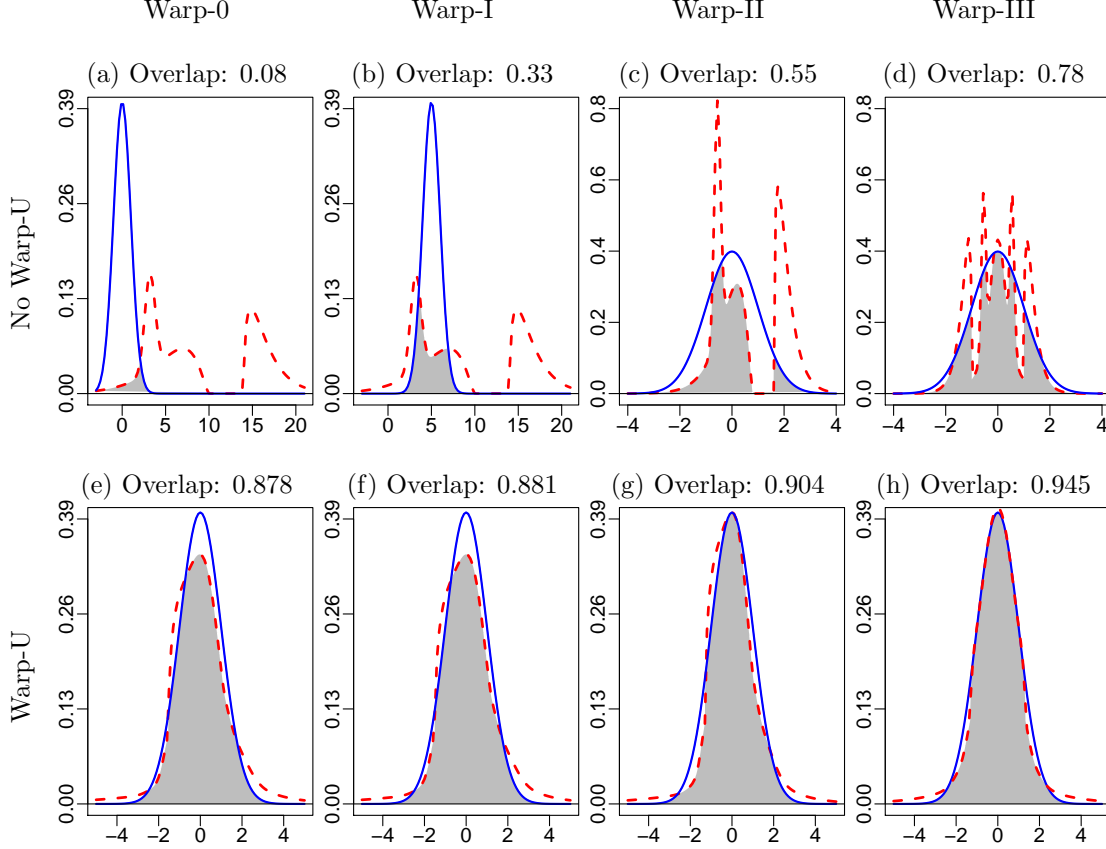


Figure 8: The two densities used in bridge sampling. Solid lines: the density of  $\mathcal{N}(0, 1)$ . Dashed lines: (a)  $p$ , density of original data  $\{w_1, \dots, w_n\}$ ; (b)  $\tilde{p}^{(I)}$ , density of Warp-I transformed data; (c)  $\tilde{p}^{(II)}$ ; (d)  $\tilde{p}^{(III)}$ ; (e)  $\tilde{p}^{(U)}$ ; (f)  $\tilde{p}^{(U+I)}$ , density after Warp-U and then Warp-I transformation; (g)  $\tilde{p}^{(U+II)}$ ; (h)  $\tilde{p}^{(U+III)}$ .

in Figure 9(b), and the RMSE reduces to 0.04. Warp-II and III transformations reduce the harmonic divergence farther, as shown in Figure 8(c,d), and the RMSE of  $\hat{\lambda}_{\text{opt}}^{(II)}$  and  $\hat{\lambda}_{\text{opt}}^{(III)}$  are also reduced, see Figure 9(c,d).

The Gaussian mixture that specifies the Warp-U transformation is shown in Figure 3 (left). The dashed curve in Figure 8(e) is the density of the Warp-U transformed data. The harmonic divergence between  $\tilde{p}^{(U)}$  and  $\phi$  reduces to 0.041, and the RMSE of  $\hat{\lambda}_{\text{opt}}^{(U)}$  is 0.009. We apply Warp-I, II, and III transformations to the Warp-U transformed data  $\tilde{w}_i^{(U)}$ , and the Harmonic divergences between the resulting densities and  $\phi$  are reduced further; see Figure 8(f-h). The Harmonic divergence between  $\phi$  and  $\tilde{p}^{(U+III)}$  is the smallest and thus  $\hat{\lambda}_{\text{opt}}^{(U+III)}$  has the smallest RMSE. It is worth mentioning that, compared with a Warp-U transformation, the further reduction due to additional warp transformations are minor when  $\phi_{\text{mix}}$  already overlaps significantly with  $p$ .

We also compare the two optimal bridge sampling estimators defined in (22) and (23), denoted as  $\hat{c}_{\text{opt}}^{(U)}$  and  $\hat{c}_{\text{opt}}^{(\text{mix})}$ . Theorem 1 implies the asymptotic variance of  $\hat{\lambda}_{\text{opt}}^{(U)}$  is smaller than that of  $\hat{\lambda}_{\text{opt}}^{(\text{mix})}$ , which is confirmed in Figure 10. In addition, the empirical evidence also supports the relationship

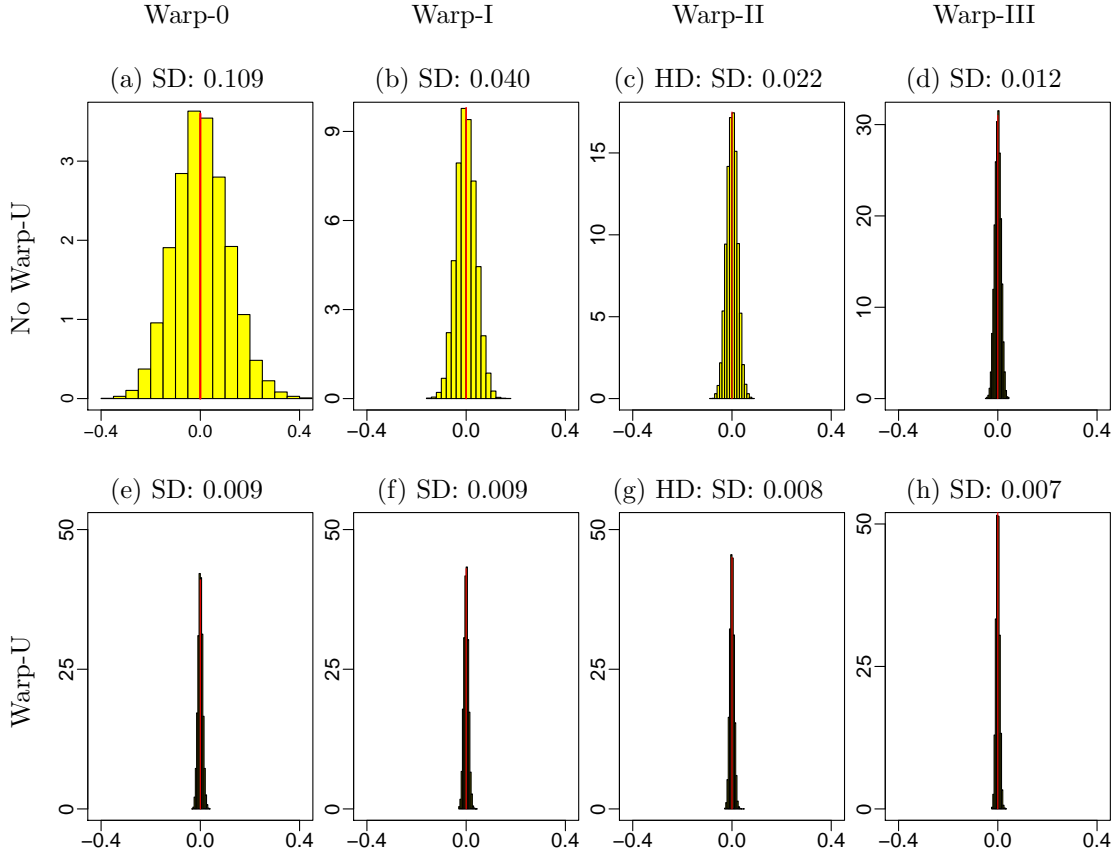


Figure 9: Histograms of  $\hat{\lambda}_{\text{opt}}^{(\mathcal{X})} - \lambda$ . (a)  $\hat{\lambda}_{\text{opt}} - \lambda$ , bridge sampling estimator with no transformation; (b)  $\hat{\lambda}_{\text{opt}}^{(\text{I})} - \lambda$ , Warp-I bridge sampling; (c)  $\hat{\lambda}_{\text{opt}}^{(\text{II})} - \lambda$ ; (d)  $\hat{\lambda}_{\text{opt}}^{(\text{III})} - \lambda$ ; (e)  $\hat{\lambda}_{\text{opt}}^{(\text{U})} - \lambda$ ; (f)  $\hat{\lambda}_{\text{opt}}^{(\text{U+I})} - \lambda$ ; (g)  $\hat{\lambda}_{\text{opt}}^{(\text{U+II})} - \lambda$ ; (h)  $\hat{\lambda}_{\text{opt}}^{(\text{U+III})} - \lambda$ .

between the asymptotic variance of  $\hat{\lambda}_{\text{opt}}$  and the harmonic divergence in (7).

## 4 Estimating Warp-U Transformation

The most crucial step in Warp-U bridge sampling is to obtain a  $\phi_{\text{mix}}$  having an adequate overlap with  $p$ , because  $\phi_{\text{mix}}$  determines the Warp-U transformations and corresponding Monte Carlo errors. In practice, we want to obtain a  $\phi_{\text{mix}}$  under reasonable constraints on computation. As mentioned in the previous section, in relatively low-dimensional ( $\leq 10$ ) problems, we can obtain a  $\phi_{\text{mix}}$  based on the expression of  $q$  (Bornkamp, 2011; Gelman et al., 2013). But these methods are too costly and unstable in high dimensions. Below we outline a simple method that can capture a good amount of the mass of  $p$ , and its computational cost is linear in the dimensionality.



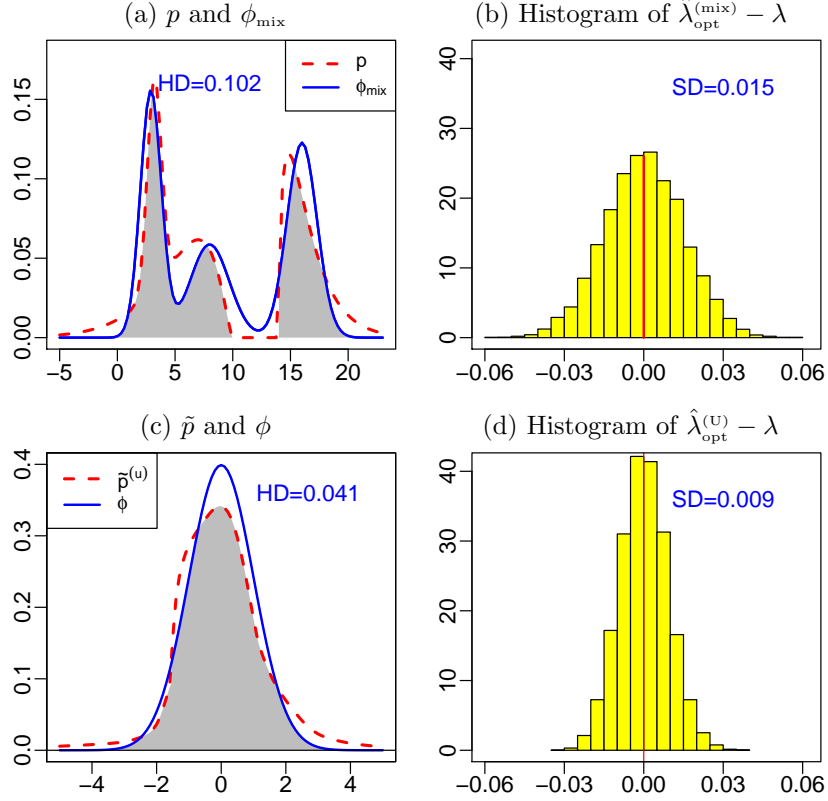


Figure 10: (a) Dashed line:  $p$ , solid line:  $\phi_{\text{mix}}$ ; (b) histogram of  $\hat{\lambda}_{\text{opt}}^{(\text{mix})} - \lambda$ ; (c) dashed line:  $\tilde{p}$ , density after Warp-U transformation, solid (nonlinear):  $\phi$ ; (d) histogram of  $\hat{\lambda}_{\text{opt}}^{(\text{U})} - \lambda$ .

#### 4.1 Fitting $\phi_{\text{mix}}$ with Diagonal Covariance Matrixes to Data

Assume we have good quality data in  $D$  dimensions from  $p$  that can represent the important regions of the density. We propose fitting the data to a mixture of normal distributions with diagonal covariance matrices, that is,

$$\phi_{\text{mix}}(\omega; \zeta) = (2\pi)^{-\frac{D}{2}} \sum_{k=1}^K \frac{\pi_k}{|\mathcal{S}_k|} \exp\left(-\frac{1}{2}(\omega - \mu_k)^\top \mathcal{S}_k^{-2}(\omega - \mu_k)\right), \quad (24)$$

where  $\pi_k$  is the weight of the normal distribution  $\mathcal{N}(\mu_k, \mathcal{S}_k^2)$ ,  $\mathcal{S}_k$  is a positive definite diagonal matrix, that is,  $\mathcal{S}_k = \text{Diag}\{\sigma_{k,1}, \sigma_{k,2}, \dots, \sigma_{k,D}\}$ , and  $\zeta = (\pi_1, \dots, \pi_K, \mu_1, \dots, \mu_K, \mathcal{S}_1, \dots, \mathcal{S}_K)$ .

Unlike in statistical inference problems where ignoring correlations can have very serious consequences, for the Warp-U transformation, using diagonal covariance matrices is a reasonable compromise between computational efficiency and Monte Carlo efficiency. As shown in previous sections, it is not a necessary requirement that  $\phi_{\text{mix}}$  must be a great fit to  $p$  before we can benefit significantly from Warp-U transformations; any  $\phi_{\text{mix}}$  with a reasonable overlap with  $p$  would do the job. In the next section, we will provide further empirical evidence to illustrate this point.

Since it is well-known that a mixture normal without suitable restrictions has unbounded

likelihood (Day, 1969; Kiefer and Wolfowitz, 1956), we estimate  $\zeta$  by the penalized MLE proposed by Chen et al. (2008). In particular, we adopt the EM approach of Chen and Tan (2009), but with a “robustified” penalty function

$$\mathbf{p}_n(\zeta) = -\frac{1}{\sqrt{n}} \sum_{k=1}^K \sum_{d=1}^D \left\{ \frac{\widehat{IQ}_d^2}{\sigma_{k,d}^2} - \log(\sigma_{k,d}^2) \right\},$$

where  $\widehat{IQ}_d$  is the inter-quantile range of the data in the  $d$ -th dimension.

Since EM tends to become trapped at local stationary points, we apply EM repeatedly for  $M$  times, each time with a different starting point  $\zeta^{(0)}$ . The initial values for  $\pi_k$ 's and  $\mathcal{S}_k$ 's are kept the same, namely  $\pi_k^{(k)} = K^{-1}$  and  $\sigma_{k,d}^2 = 1.5\widehat{IQ}_d^2$  for all  $k$ . For the mean parameters  $\mu_k$ , for the first  $M/2$  replications, we randomly draw  $K$  points without replacement from the available data as their initial values. For the second  $M/2$  replications, along the dimension with the largest estimated variance, we first divide the region where 95% of the data reside in  $K$  subregions so that each subregion contains approximately the same number of data points. We then sample one data point from each of the  $K$  subregions as the initial mean parameters. The stopping criterion is set to satisfy  $|1 - (l_n^{(t)}/l_n^{(t-1)})| < 10^{-6}$ , where  $l_n^{(t)}$  is the value of the (un-penalized) log-likelihood at iteration  $t$ . In our simulations, EM stopped mostly within 100 iterations. After obtaining  $M$  estimates of  $\zeta$ , we choose the one with the largest likelihood value as our parameter,  $\tilde{\zeta}$ , for Warp-U bridge sampling. Simulations show that  $M$  as small as 2 to 10 is sufficient to obtain a local maxima that serves well for the purpose of ensuring adequate amount of overlap between  $p$  and  $\phi_{\text{mix}}$ .

## 4.2 Overcoming Adaptive Bias

Let  $\tilde{\zeta}_D$  be the estimate of  $\zeta$  via the EM approach applied to the whole dataset,  $D = \{w_1, \dots, w_n\}$ , from  $p$ , and  $\hat{\lambda}_D^{(U)} = \log(\hat{c}_D^{(U)})$  as the corresponding Warp-U bridge sampling estimator. Because  $\tilde{\zeta}_D$  is a function of the data, the distribution of the corresponding Warp-U transformed data,  $\{\tilde{w}_1, \dots, \tilde{w}_n\}$ , is no longer proportional to  $\tilde{q}(\cdot; \zeta)$  of (21), even or especially at  $\zeta = \tilde{\zeta}_D$ . Consequently, an adaptive bias in  $\hat{\lambda}_D^{(U)}$  is induced by the dependence of  $\tilde{\zeta}_D$  on  $D$ , as demonstrated in Figure 11, which also illustrates the (little) impact of knowingly using simplified (and hence misspecified) covariance matrices.

Specifically, Figure 11 compares four Warp-U bridge sampling estimators with the optimal choice of  $\alpha$ , denoted by  $\hat{\lambda}_{D,\text{Diag}}^{(U)}$ ,  $\hat{\lambda}_{D,\text{Full}}^{(U)}$ ,  $\hat{\lambda}_{I,\text{Diag}}^{(U)}$ , and  $\hat{\lambda}_{I,\text{Full}}^{(U)}$ , where the first subscript specifies whether  $\zeta$  is estimated from the whole data set (D) or from an independent data set (I), and the second subscript indicates whether the covariance matrices in  $\phi_{\text{mix}}$  are restricted to diagonal (Diag) or not (Full). The density  $p$  is a mixture of 25 multivariate skew-t distributions, obtained using the function *dmst* (density of multivariate skew-t) in the R package ‘sn’. The 25 skew-t distributions have degrees of freedom varying from 1 to 4, skew parameters alpha varying from -100 to 200,

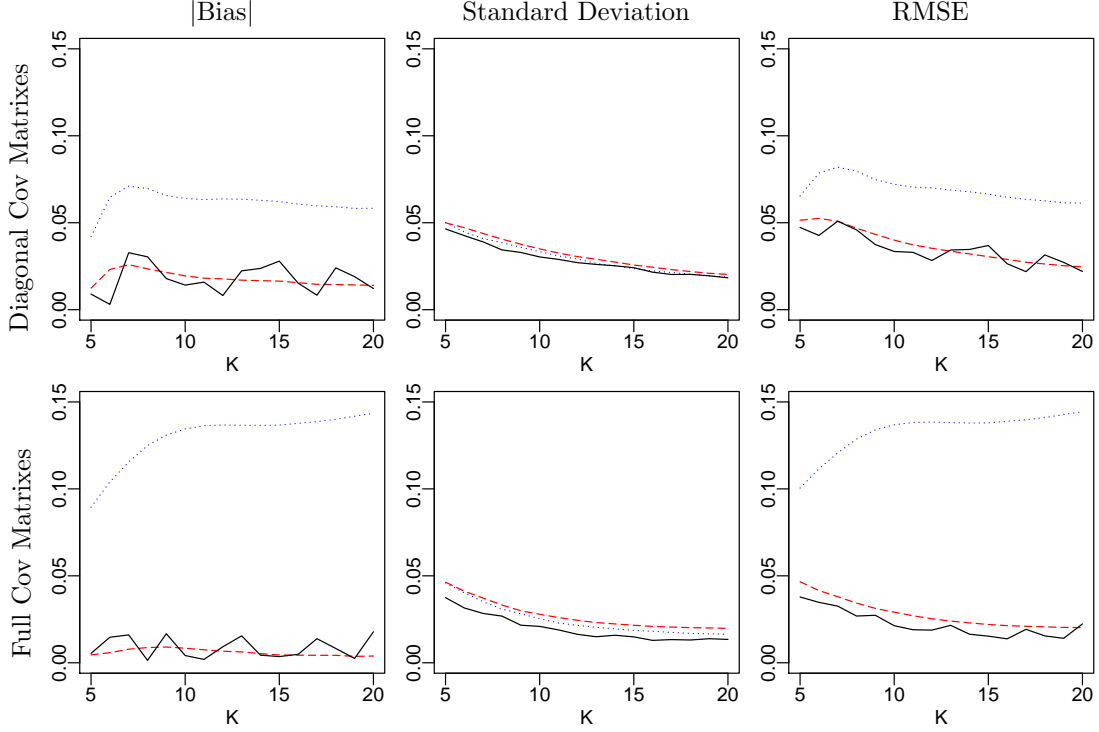


Figure 11: The columns show the absolute bias, the standard deviation, and the RMSE of (i)  $\hat{\lambda}_{D,\mathcal{Z}}^{(U)} = \log(\hat{c}_{D,\mathcal{Z}}^{(U)})$  (dotted lines), the Warp-U estimator specified by  $\tilde{\zeta}_D$ , which is estimated from  $D = \{w_1, \dots, w_n\}$ , (ii)  $\hat{\lambda}_{I,\mathcal{Z}}^{(U)} = \log(\hat{c}_{I,\mathcal{Z}}^{(U)})$  (solid lines), Warp-U specified by  $\tilde{\zeta}_I$ , which is independent of  $D$ , and (iii) (dashed lines) the average of two Warp-U bridge sampling estimators with half of data for estimating  $\zeta$  and the other half for bridge sampling. The subscript “ $\mathcal{Z}$ ” represents “Diag” (top row) or “Full” (bottom row) for the covariance matrices in the Gaussian mixture model.

and none of the scale matrices Omega is sparse; see Azzalini (2011, 2013) for details.

The number of components in  $\phi_{\text{mix}}$ , which determines the Warp-U transformation, varies from 5 to 20. We simulate  $10^4$  replicate datasets, each of which contains 2500 independent draws from  $p$  and 2500 independent draws from  $\mathcal{N}(0, I_{10})$ . For each  $K$  and each type of covariance matrices, we obtain  $\tilde{\zeta}_I$  by maximizing the penalized log-likelihood based on a fixed dataset from  $p$  that is independent of any data used for bridge sampling. The resulting  $\hat{\lambda}_{I,\text{Diag}}^{(U)}$  and  $\hat{\lambda}_{I,\text{Full}}^{(U)}$  serve as our benchmark for comparison because they are not subject to the adaptive bias.

Figure 11 shows the summary statistics of  $\hat{\lambda}_{\mathcal{Y},\text{Diag}}^{(U)}$  (top row) and  $\hat{\lambda}_{\mathcal{Y},\text{Full}}^{(U)}$  (bottom row), where the subscript “ $\mathcal{Y}$ ” represents “D” or “I”. The dotted and solid lines in the figure correspond to  $\hat{\lambda}_{D,\mathcal{Z}}^{(U)}$  and  $\hat{\lambda}_{I,\mathcal{Z}}^{(U)}$ , respectively, where “ $\mathcal{Z}$ ” indexes “Diag” or “Full”. The first column in Figure 11 shows the excessive bias of  $\hat{\lambda}_{D,\mathcal{Z}}^{(U)}$  compared with  $\hat{\lambda}_{I,\mathcal{Z}}^{(U)}$ . We see that, as  $K$  increases, the Gaussian mixture model,  $\phi_{\text{mix}}(\cdot; \tilde{\zeta}_I)$ , while achieving a better fit to the fixed dataset, does not necessarily result in smaller bias, hence the zigzag shape of the bias of  $\hat{\lambda}_{I,\mathcal{Z}}^{(U)}$ . The second column shows that the variance of  $\hat{\lambda}_{D,\mathcal{Z}}^{(U)}$  and that of  $\hat{\lambda}_{I,\mathcal{Z}}^{(U)}$  are quite similar. The variance decreases as  $K$  increases,

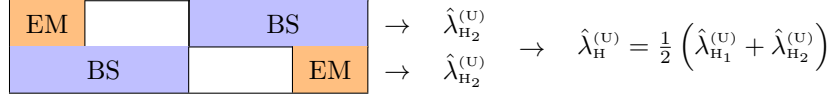


Figure 12: A proposed solution to remove the adaptive bias without (unduly) increasing the variance of the Warp-U bridge sampling estimator. Each  $\hat{\lambda}_{H_i}^{(U)}$ ,  $i = 1, 2$  is obtained by using a part of 50% of the data for estimating  $\zeta$  and the other 50% for Warp-U bridge sampling. We then average the two estimators.

because on average larger  $K$  corresponds to more overlap between  $p$  and the calibrated  $\phi_{\text{mix}}$ , and thus more overlap between  $\tilde{p}$  and  $\phi$ . In addition,  $\hat{\lambda}_{i,z}^{(U)}$  has slightly smaller variance than  $\hat{\lambda}_{D,z}^{(U)}$  for fixed  $K$ , because  $\tilde{\zeta}_i$  is estimated from a much larger dataset than  $\tilde{\zeta}_D$ . The last column in Figure 11 shows the RMSE of  $\hat{\lambda}_{D,z}^{(U)}$  is dominated by the bias term, much larger than that of  $\hat{\lambda}_{i,z}^{(U)}$ .

Since the additional bias of  $\hat{\lambda}_{D,z}^{(U)}$  is due to the dependence of  $\tilde{\zeta}_D$  on the data coming from  $p$ , an obvious remedy is to use two independent subsets from  $p$  for estimating  $\zeta$  and for bridge sampling. We can then switch the roles of these subsets to ensure statistical efficiency. Figure 12 depicts our sub-sampling strategy, obtaining two separate bridge sampling estimators,  $\hat{\lambda}_{H_i}^{(U)}$ ,  $i = 1, 2$ . Each  $\hat{\lambda}_{H_i}^{(U)}$  is obtained by using  $L \leq n/2$  of draws from  $p$  to estimate  $\zeta$  and the other 50% draws for the Warp-U bridge sampling specified by the estimated  $\zeta$ . The final estimator  $\hat{\lambda}_H^{(U)}$  is the average of  $\hat{\lambda}_{H_1}^{(U)}$  and  $\hat{\lambda}_{H_2}^{(U)}$ . Empirical studies have shown the correlation of  $\hat{\lambda}_{H_1}^{(U)}$  and  $\hat{\lambda}_{H_2}^{(U)}$  is very small (mostly  $< 0.06$ ; see Figure 14), thus, the variance of  $\hat{\lambda}_H^{(U)}$  is nearly half of the variance of  $\hat{\lambda}_{H_i}^{(U)}$ . The dashed lines in Figure 11 show the bias, the standard deviation, and the RMSE of  $\hat{\lambda}_{H,\text{Diag}}^{(U)}$  (top row) and  $\hat{\lambda}_{H,\text{Full}}^{(U)}$  (bottom row), which are very close to their corresponding benchmarks (solid lines).

Figure 11 also demonstrates that once the adaptive bias is removed, whether to use full or diagonal covariance matrices for fitting  $\phi_{\text{mix}}$  makes minor differences in terms of estimation errors, as seen by comparing the solid lines, or dashed lines, between the top and bottom plots in each column. But fitting with full covariance matrices is computationally much more expensive.

To demonstrate, Figure 13 (left) shows the log of RMSE of  $\hat{\lambda}_{I,\text{Diag}}^{(U)}$ ,  $\hat{\lambda}_{I,\text{Full}}^{(U)}$ ,  $\hat{\lambda}_{H,\text{Diag}}^{(U)}$ , and  $\hat{\lambda}_{H,\text{Full}}^{(U)}$ . On average,  $\log(\text{RMSE})$  of  $\hat{\lambda}_{I,\text{Diag}}^{(U)}$  (thin solid line) is about 50% larger than that of  $\hat{\lambda}_{I,\text{Full}}^{(U)}$  (thick solid line). However,  $\log(\text{RMSE})$  of  $\hat{\lambda}_{H,\text{Diag}}^{(U)}$  (thin dashed line) is only 16.7% larger than that of  $\hat{\lambda}_{H,\text{Full}}^{(U)}$  (thick dashed line), and their difference diminishes as  $K$  increases. This is because, when  $K$  is large, over-fitting becomes more serious for the full-matrix model due to the additional  $KD(D-1)/2$  parameters in the model. The diagonal-matrix model, being much more parsimonious, continues to fit the data better and the resulting RMSE decreases at a stable rate.

Figure 13 (right) shows the CPU seconds for estimating  $\zeta$  via the EM algorithm. On average in this study, it takes 12 times longer to obtain  $\phi_{\text{mix}}$  with full covariance matrices than with diagonal covariance matrices, and the difference increases with the dimension. In addition, in the step of bridge sampling, evaluating  $\phi_{\text{mix}}$  with full covariance matrices is much more costly than with diagonal covariance matrices. Therefore, a small loss of statistical efficiency but huge

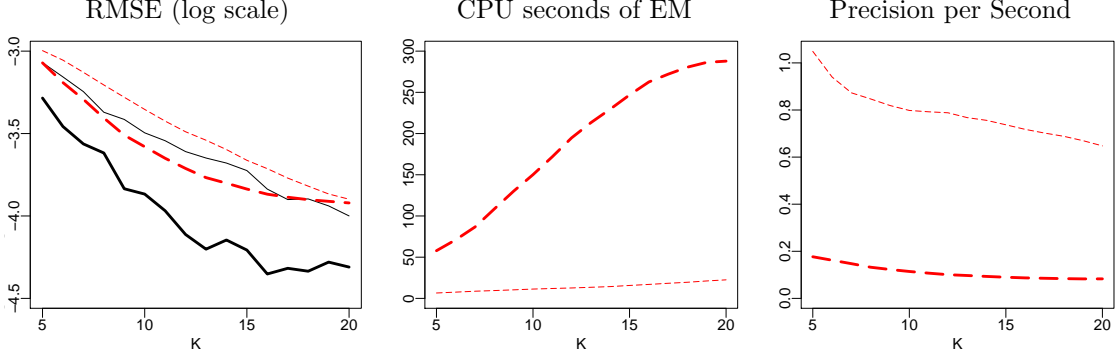


Figure 13: (Left) RMSE (on a logarithmic scale) of different estimators; (middle) CPU seconds of each EM algorithm; (right) Precision per CPU second defined as  $(1/\text{MSE})/\text{time}$ . (Solid lines) Warp-U bridge sampling with  $\tilde{\zeta}_1$ ; (dashed lines) the average of the two Warp-U bridge sampling estimators with half of data used for estimating  $\zeta$  and the other half for bridge sampling. (Thin lines) the covariance matrices are diagonal matrices; (thick lines) the covariance matrices are not restricted to diagonal matrices.

gain in computational efficiency justifies the use of diagonal covariance matrices. Our empirical evidence suggests that, for reducing RMSE, increasing the number of mixture components  $K$  is more effective than to use full covariance matrices. This is consistent with the intuition that, for the purposes of increasing distributional overlaps, it is more important to increase the chance for our model to find locations of (major) modes than to refine the curvature estimation (e.g., to better orient directions) at the estimated modes.

Therefore, in the subsequent sections, we only consider  $\phi_{\text{mix}}$  fitted with diagonal covariance matrices. For simplicity, we drop the subscripts ‘‘H’’ and ‘‘Diag’’, and let  $\hat{\lambda}_{\alpha,1}^{(x)}$  and  $\hat{\lambda}_{\alpha,2}^{(x)}$  denote the estimators with half of the data used for estimating  $\zeta$  and the other half in bridge sampling, and the combined estimator as  $\hat{\lambda}_{\alpha}^{(x)} = \frac{1}{2} (\hat{\lambda}_{\alpha,1}^{(x)} + \hat{\lambda}_{\alpha,2}^{(x)})$ .

### 4.3 Approximating Estimation Uncertainties

For  $L \leq n/2$ , let  $\{w_1, \dots, w_L\}$  be  $L$  i.i.d draws from  $p$  we use to estimate  $\zeta$ , resulting in  $\tilde{\zeta}_L$ . Specified by the estimate  $\tilde{\zeta}_L$ , we apply the corresponding Warp-U transformation to the other half of data  $W_{n/2} \equiv \{w_{1+n/2}, \dots, w_n\} \stackrel{iid}{\sim} p$ . Let  $\hat{\lambda}_{\alpha,1}^{(U)} = \hat{\lambda}_{\alpha,1}^{(U)}(\tilde{\zeta}_L)$  be the bridge sampling estimator based on  $Z_{m/2} \equiv \{z_{1+m/2}, \dots, z_m\} \stackrel{iid}{\sim} \phi$  and the Warp-U transformed data,  $\{\tilde{w}_{1+n/2}, \dots, \tilde{w}_n\} \stackrel{iid}{\sim} \tilde{p}$ . Then by the law of total variance,

$$\text{Var} \left( \hat{\lambda}_{\alpha,1}^{(U)} \right) = \text{E}_L \left[ \text{Var} \left( \hat{\lambda}_{\alpha,1}^{(U)} | \tilde{\zeta}_L \right) \right] + \text{Var}_L \left[ \text{E} \left( \hat{\lambda}_{\alpha,1}^{(U)} | \tilde{\zeta}_L \right) \right],$$

where  $\text{E}_L$  and  $\text{Var}_L$  are taken over the sampling distribution of  $\tilde{\zeta}_L$ . Now because  $\tilde{\zeta}_L$  is independent of  $\{W_{n/2}, Z_{m/2}\}$ , any conditional moment of  $\hat{\lambda}_{\alpha,1}^{(U)}$  given  $\tilde{\zeta}_L$  is the same as that of  $\hat{\lambda}_{\alpha,1}^{(U)}(\zeta)$ ,

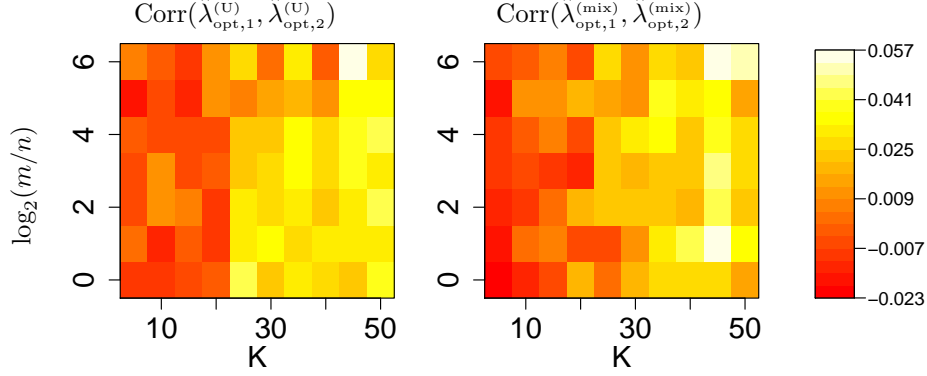


Figure 14: The correlation between  $\hat{\lambda}_{opt,1}^{(x)}$  and  $\hat{\lambda}_{opt,2}^{(x)}$  with different  $K$  and  $m/n$ .

but with  $\zeta$  evaluated at  $\tilde{\zeta}_L$ . From Meng and Wong (1996), we have

$$\text{Var}\left(\hat{\lambda}_{\alpha,1}^{(u)}(\zeta)\right)\Big|_{\zeta=\tilde{\zeta}_L} = \frac{2}{n+m}\mathcal{V}_{\alpha}(\tilde{p}, \phi) + o\left(\frac{1}{n+m}\right), \quad (25)$$

where  $\mathcal{V}_{\alpha}(\tilde{p}, \phi)$  is defined in (3), and the asymptotic bias of  $\hat{\lambda}_{\alpha,1}^{(u)}(\zeta)$  is of the order  $(m+n)^{-1}$ . Consequently,

$$\text{Var}\left(\hat{\lambda}_{\alpha,1}^{(u)}\right) = \frac{2}{n+m}E_L[\mathcal{V}_{\alpha}(\tilde{p}, \phi)] + o\left(\frac{1}{n+m}\right). \quad (26)$$

Figure 14 (left) shows the correlation between  $\hat{\lambda}_{opt,1}^{(u)}$  and  $\hat{\lambda}_{opt,2}^{(u)}$  for different values of  $K$  and  $m$ , based on  $10^4$  replications, within each of which  $n = 10^4$  data points are generated from  $p$ , as described in Section 4.2. The correlation between  $\hat{\lambda}_{opt,1}^{(u)}$  and  $\hat{\lambda}_{opt,2}^{(u)}$  is due to the fact that  $L = 50K$  data points used in bridge sampling for one estimator are used for estimating  $\zeta$  for the other estimator, thus we observe the correlation increases with  $K$ . Figure 14 (left) shows the correlation is very small ( $< 0.06$ ) even when  $K = 50$ , so practically we can take

$$\text{Var}\left(\hat{\lambda}_{\alpha}^{(u)}\right) \approx \frac{1}{2}\text{Var}\left(\hat{\lambda}_{\alpha,i}^{(u)}\right) = \frac{1}{n+m}E_L[\mathcal{V}_{\alpha}(\tilde{p}, \phi)] + o\left(\frac{1}{n+m}\right). \quad (27)$$

For a given  $\tilde{\zeta}_L$ , to estimate  $\text{Var}\left(\hat{\lambda}_{\alpha,1}^{(u)}|\tilde{\zeta}_L\right)$ , we divide  $\{\tilde{w}_{1+n/2}, \dots, \tilde{w}_n\}$  and  $\{z_{1+m/2}, \dots, z_m\}$  each into  $S \geq 2$  non-overlapping subsets of equal size, and obtain  $S$  separate estimators  $\hat{\lambda}_{\alpha,1,s}^{(u)}$ , for  $s = 1, \dots, S$ . The evaluations of  $\tilde{q}$  and  $\phi$  at these data points are already done when computing  $\hat{\lambda}_{\alpha,1}^{(u)}$ , so little additional computation is required to compute  $\hat{\lambda}_{\alpha,1,s}^{(u)}$ . The empirical variance of  $\{\hat{\lambda}_{\alpha,1,s}^{(u)}; s = 1, \dots, S\}$ , denoted as  $\hat{\nu}_{\alpha,1}^{(u)}$ , estimates the variance of the bridge sampling estimator with  $n/(2S)$  data points from  $\tilde{p}$  and  $m/(2S)$  data points from  $\phi$ . Therefore  $\mathcal{V}_{\alpha}(\tilde{p}, \phi)$  in (3) can be estimated by  $(n+m)\hat{\nu}_{\alpha,1}^{(u)}/(2S)$ , and similarly, by symmetry, by its second-half counterpart  $(n+m)\hat{\nu}_{\alpha,2}^{(u)}/(2S)$ , where  $\hat{\nu}_{\alpha,2}^{(u)}$  is the empirical variance of  $\hat{\lambda}_{\alpha,2,s}^{(u)}$ . Consequently, by (27),  $\text{Var}\left(\hat{\lambda}_{\alpha}^{(u)}\right)$  can be approximated by

$$\hat{\nu}_{\alpha}^{(u)} = \frac{1}{2}\frac{\hat{\nu}_{\alpha,1}^{(u)} + \hat{\nu}_{\alpha,2}^{(u)}}{2S} = \frac{1}{4S(S-1)}\sum_{i=1}^2\sum_{s=1}^S\left(\hat{\lambda}_{\alpha,i,s}^{(u)} - \bar{\lambda}_{\alpha,i}^{(u)}\right)^2, \quad (28)$$

where  $\bar{\lambda}_{\alpha,i}^{(U)} = \sum_{s=1}^S \hat{\lambda}_{\alpha,i,s}^{(U)}/S$ . There is a trade-off in choosing  $S$ , because small  $S$  may cause inaccurate estimation of the variance by  $\hat{v}_{\alpha,1}^{(U)}$  and  $\hat{v}_{\alpha,2}^{(U)}$ , whereas large  $S$  may break the asymptotic results in (27) we rely on to obtain  $\text{Var}\left(\hat{\lambda}_{\alpha,i,s}^{(U)}|\tilde{\zeta}_L\right) \approx \frac{2S}{n+m}\mathcal{V}_\alpha(\tilde{p},\phi)$ .

Similarly, for the bridge sampling estimator based directly on  $\{w_{1+n/2}, \dots, w_n\} \stackrel{iid}{\sim} p$  and  $\{x_{1+m/2}, \dots, x_m\} \stackrel{iid}{\sim} \phi_{\text{mix}}(\cdot; \tilde{\zeta}_L)$ , that is,  $\hat{\lambda}_{\alpha,1}^{(\text{mix})}$ , we have

$$\text{Var}\left(\hat{\lambda}_{\alpha,1}^{(\text{mix})}\right) = \frac{2}{n+m}E_L[\mathcal{V}_\alpha(p, \phi_{\text{mix}})] + o\left(\frac{1}{n+m}\right),$$

and the variance of  $\hat{\lambda}_\alpha^{(\text{mix})} = (\hat{\lambda}_{\alpha,1}^{(\text{mix})} + \hat{\lambda}_{\alpha,2}^{(\text{mix})})/2$  is approximately half of  $\text{Var}\left(\hat{\lambda}_{\alpha,1}^{(\text{mix})}\right)$  when  $\text{Corr}(\hat{\lambda}_{\alpha,1}^{(\text{mix})}, \hat{\lambda}_{\alpha,2}^{(\text{mix})})$  can be ignored, as indicated in the right plot of Figure 14. Moreover,  $\text{Var}\left(\hat{\lambda}_{\alpha,1}^{(\text{mix})}\right)$  can be estimated in the same way as in (28), with the subscript ‘‘U’’ replaced by ‘‘MIX’’. For fixed  $\tilde{\zeta}_L$ , Theorem 1 implies  $\mathcal{V}_\alpha(p, \phi_{\text{mix}}) \leq \mathcal{V}_\alpha(\tilde{p}, \phi)$  (at least) for the geometric bridge and optimal bridge, and hence in general we expect the Warp-U bridge sampling estimators to dominate the original bridge sampling estimators, as we shall demonstrate in the next section.

## 5 Computational Configurations and Considerations

In the algorithm to obtain  $\hat{\lambda}_\alpha^{(x)}$ , there are three tuning parameters:

- $K$ : the number of components in the Gaussian mixture model  $\phi_{\text{mix}}(\cdot; \zeta)$ ;
- $L$ : the number of data points from  $p$  to estimate  $\zeta$ , as long as  $L \leq n/2$ ;
- $m$ : the sample size of the dataset sampled from  $N(0, I_D)$  or  $\phi_{\text{mix}}$ .

To reach a sensible compromise between statistical and computational efficiencies, our criterion for comparisons will be the precision per CPU second ( $PpS$ ), that is,  $(\text{Var} \times \text{CPU seconds})^{-1}$ . We compare  $\hat{\lambda}_{\text{opt}}^{(U)} = \frac{1}{2}\left(\hat{\lambda}_{\text{opt},1}^{(U)} + \hat{\lambda}_{\text{opt},2}^{(U)}\right)$  and  $\hat{\lambda}_{\text{opt}}^{(\text{mix})} = \frac{1}{2}\left(\hat{\lambda}_{\text{opt},1}^{(\text{mix})} + \hat{\lambda}_{\text{opt},2}^{(\text{mix})}\right)$ , with different choices of  $(K, L, m)$ , in searching for practical guidance for choosing these tuning parameters. In the simulation, we set the sample size  $n$  to be  $10^4$  in order to investigate the impact of large  $K$  on the estimators. For each  $(K, L, m)$ , we summarize the estimates from the entire algorithm applied to each of the  $10^4$  replicate datasets from  $p$ , which is the same as the 10-dimensional example in Section 4.2. If not specified,  $L = \min(50K, n/2)$  and  $m = n$ .

### 5.1 Impact of $K$

Figure 15 explains why the variance and the RMSE of  $\hat{\lambda}_{\text{opt}}^{(U)}$  in Figure 11 decrease as  $K$  increases. The dotted line is the average of the maximum log-likelihood  $\bar{l}_{\text{fit}}$ , defined as

$$\bar{l}_{\text{fit}} = \frac{1}{L} \sum_{i=1}^L \log\left(\phi_{\text{mix}}(w_i; \tilde{\zeta}_L)\right),$$

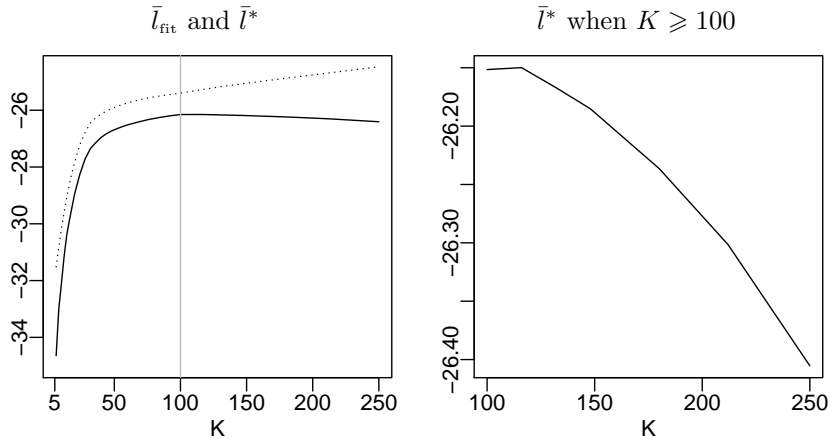


Figure 15: (Dotted line)  $\bar{l}_{\text{fit}}$ ; (solid lines)  $\bar{l}^*$ . The gray vertical line marks the value of  $K$ , around which  $\bar{l}^*$  changes from increasing to decreasing as  $K$  increases. The figure on the right-hand side shows  $\bar{l}^*$  for  $K$  ranging from 100 to 250 (but notice the scale change on the vertical axis).

where  $\{w_1, \dots, w_L\}$  are used for estimating  $\zeta$  via the EM algorithm. It measures how well the calibrated  $\phi_{\text{mix}}$  fits to the  $L$  data points used for estimating  $\zeta$ , so  $\bar{l}_{\text{fit}}$  is an increasing function of  $K$ . The solid line in Figure 15 represents the average log-likelihood  $\bar{l}^*$  based on the other half of the data and evaluated at  $\tilde{\zeta}_L$ , i.e.,

$$\bar{l}^* = \frac{2}{n} \sum_{i=n/2+1}^n \log \left( \phi_{\text{mix}}(w_i; \tilde{\zeta}_L) \right).$$

It can be viewed as a “predictive divergence” of the fitted  $\phi_{\text{mix}}$  from  $p$ . For moderate  $K$ , on average, as the mixture model fits the  $L$  data points better, more mass of  $p$  is captured by the calibrated  $\phi_{\text{mix}}$ , and thus both  $\bar{l}^*$  and the statistical efficiency of  $\hat{\lambda}_{\text{opt}}^{(U)}$  increases as  $K$  increases.

However, for a large  $K$ , the Gaussian mixture model will overfit the  $L \leq n/2$  data points from  $p$ . Figure 15 (right) shows that  $\bar{l}^*$  decreases slightly when  $K$  exceeds 100, indicating a slight increase of the divergence between  $p$  and  $\phi_{\text{mix}}(\cdot; \tilde{\zeta}_L)$ . Figure 16 shows the |bias|, standard deviation, and the RMSE (on a logarithmic scale) of  $\hat{\lambda}_{\text{opt}}^{(U)}$  (solid lines) and  $\hat{\lambda}_{\text{opt}}^{(\text{mix})}$  (dashed lines), with  $K$  ranging from 5 to 250. When  $K$  exceeds  $n/100$ , there is a slight increase in both the variance and the RMSE of these estimators as  $K$  continues to increase.

Figure 17 (left) shows the computational cost of  $\hat{\lambda}_{\text{opt}}^{(U)}$  (solid line) and  $\hat{\lambda}_{\text{opt}}^{(\text{mix})}$  (dashed line). When  $K > n/100$ , the total CPU time  $T_{\text{opt}}^{(U)}$  exhibits a quadratic growth with  $K$ , whereas  $T_{\text{opt}}^{(\text{mix})}$  grows linearly with  $K$ . Since there is little gain in statistical efficiency when increasing  $K$  beyond  $n/100$ , the additional computational cost is wasted. Figure 17 (right) plots the  $PpS$ . The largest  $PpS$  is obtained when  $K$  is between 20 and 30.

Based on our simulation, a rule of thumb in choosing  $K$  is  $K \leq n/100$  to avoid overfitting to the  $L$  data points and unnecessary computational cost. Beyond that, we have not been able to obtain any simple rule for specifying the optimal  $K$ . We want  $K$  not too small to induce



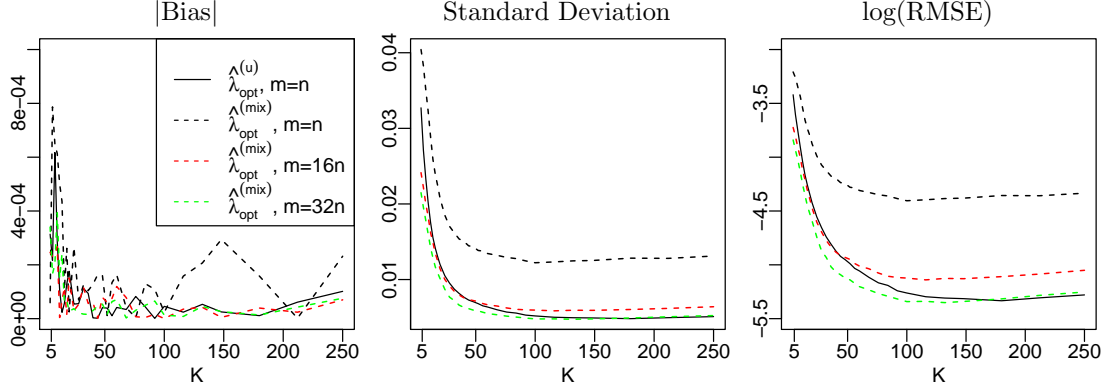


Figure 16: The three columns show  $|\text{bias}|$ , standard deviation and  $\log(\text{RMSE})$  of  $\hat{\lambda}_{\text{opt}}^{(u)}$  (solid lines) and  $\hat{\lambda}_{\text{opt}}^{(\text{mix})}$  (dashed lines). Different colors correspond to different values of  $m$  in the estimators. Black:  $m = n$ ; Red:  $m = 16n$ ; Green:  $m = 32n$ .

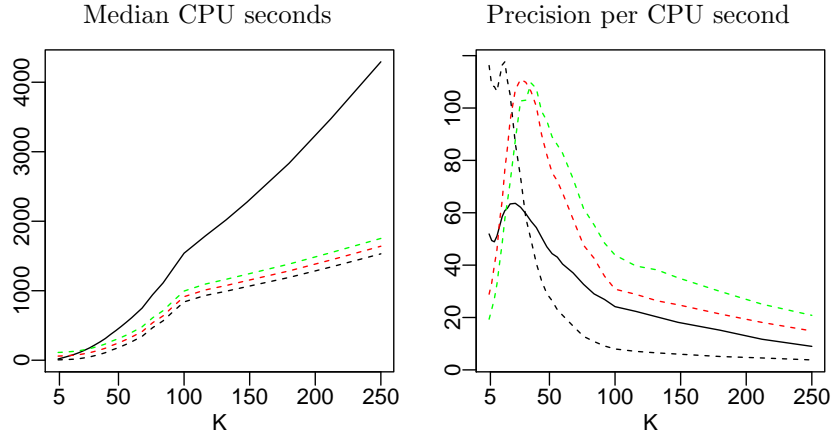


Figure 17: The total computational cost  $T_{\text{opt}}^{(x)}$  (left), and the precision per CPU second (right) of the optimal bridge sampling estimators  $\hat{\lambda}_{\text{opt}}^{(u)}$  (solid lines,  $m = n$ ) and  $\hat{\lambda}_{\text{opt}}^{(\text{mix})}$  (dashed lines) with  $m = n$  (black),  $16n$  (red), and  $32n$  (green).

sufficient overlap between  $\phi$  and  $\tilde{p}$ , but not too large to control the computational cost, both of which require problem specific knowledge. But as discussed before, the beauty of Warp-U bridge sampling is that it does *not* rely on  $\phi_{\text{mix}}$  to be a great fit to  $p$  to produce very good estimators.

## 5.2 Impact of $L$

Other factors being fixed, on average, larger  $L$  results in more overlap between  $p$  and  $\phi_{\text{mix}}$ , hence more overlap between  $\tilde{p}$  and  $\phi$ , and better statistical efficiency of  $\hat{\lambda}_{\alpha}^{(u)}$ . Therefore, if we are not concerned about the computational cost, we should use all of the data points in one half of the dataset to estimate  $\zeta$ , and to apply the corresponding Warp-U transformation to the other half of the dataset, in order to obtain  $\hat{\lambda}_{\alpha,i}^{(u)}$ , for  $i = 1, 2$ . However, unless  $p$  is already a Gaussian

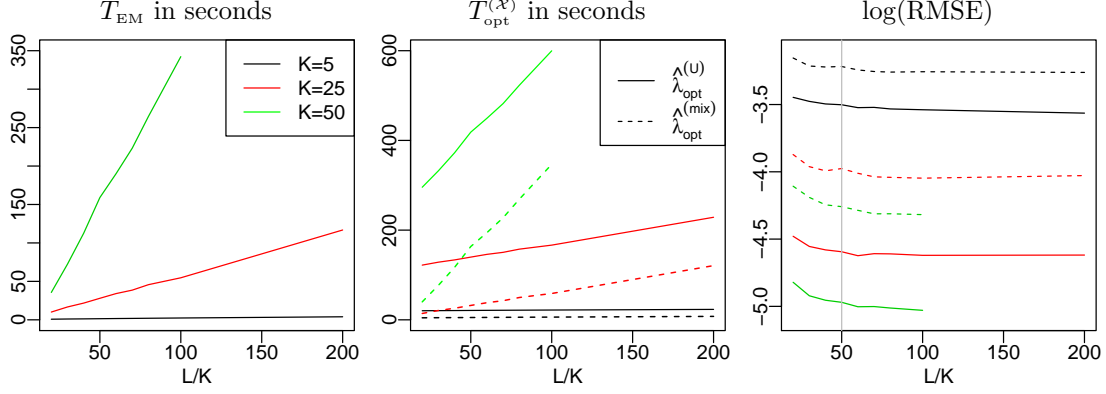


Figure 18: The impact of  $L$  on  $T_{EM}$  (left),  $T_{opt}^{(X)}$  (middle), and the RMSE of  $\hat{\lambda}_{opt}^{(X)}$  (right). Black lines:  $K = 5$ ; red lines:  $K = 25$ ; green lines:  $K = 50$ . When  $K = 50$ , we can take  $L/K$  only up to 100, because  $L \leq n/2$ .

mixture as specified in (24), letting  $L \rightarrow \infty$  does not guarantee any  $f$ -divergence between  $p$  and  $\phi_{\text{mix}}(\cdot; \tilde{\zeta}_L)$  to vanish. Hence choosing a large  $L$  may only incur diminishing return.

Figure 18 shows the impact of  $L$  on (i)  $T_{EM}$ , the computational cost in estimating  $\phi_{\text{mix}}$ , (ii)  $T_{opt}^{(U)}$  and  $T_{opt}^{(mix)}$ , the total computational cost in obtaining  $\hat{\lambda}_{opt}^{(U)}$  and  $\hat{\lambda}_{opt}^{(mix)}$ , and (iii) the RMSE. The size of the sample for estimating  $\zeta$  should be linear in  $K$ , so we compare estimators with different values of  $L/K$ . Since  $L$  affects only the step of estimating  $\zeta$ , for fixed  $K$ , both  $T_{EM}$  and  $T_{opt}^{(X)}$  grow linearly with  $L$ . In terms of the statistical efficiency, for a fixed  $K$ , having more data to estimate  $\zeta$  on average results in more overlap between  $p$  and  $\phi_{\text{mix}}(\cdot; \tilde{\zeta}_L)$ . Figure 18 (right) shows that RMSE decreases as  $L/K$  increases, but the reduction rate becomes very small when  $L/K > 50$ . Later Figure 22 shows a similar effect in a 50-dimension example. A reasonable quick rule of thumb is then to set  $L = \min(50K, n/2)$ .

### 5.3 Impact of $m$ and a Comparison of $\hat{\lambda}_{opt}^{(mix)}$ and $\hat{\lambda}_{opt}^{(U)}$

Similar to  $K$  and  $L/K$ , larger  $m$  improves the precision of the estimators but increases the computational cost. Figure 19 (left) shows that both  $T_{opt}^{(U)}$  (solid lines) and  $T_{opt}^{(mix)}$  (dashed lines) grow linearly as  $m$  increases from  $n$  to  $64n$ . Figure 19 (middle) shows that the standard deviation of  $\hat{\lambda}_{opt}^{(X)}$  is inversely related to  $m$ .

Consistent with our theoretical results, Figures 16, 18, and 19 all illustrate that, for the same  $(K, L, m)$ ,  $\hat{\lambda}_{opt}^{(U)}$  has better statistical efficiency than  $\hat{\lambda}_{opt}^{(mix)}$ , but  $\hat{\lambda}_{opt}^{(U)}$  is computationally much more costly than  $\hat{\lambda}_{opt}^{(mix)}$ . Figure 16 (middle) shows that the difference between the variances of  $\hat{\lambda}_{opt}^{(U)}$  and  $\hat{\lambda}_{opt}^{(mix)}$  increases as  $K$  increases. A possible explanation is as follows. In the Warp-U transformation, the overlap of  $\tilde{p}^{(k)}$  and  $\tilde{\phi}^{(k)}$  remains the same as that of  $p^{(k)}$  and  $\phi^{(k)}$ , and the additional overlap comes from rematching  $\tilde{p}^{(k)}$  with the remainder of  $\tilde{\phi}^{(j)}$  (for  $j \neq k$ ) that does

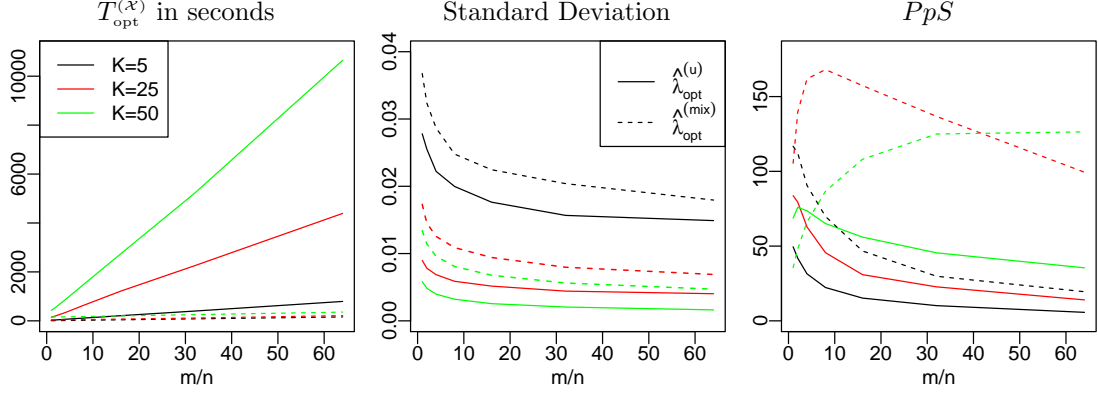


Figure 19: The total CPU time  $T_{\text{opt}}^{(x)}$  (left), the standard deviation (middle), and the  $PpS$  of  $\hat{\lambda}_{\text{opt}}^{(u)}$  (solid lines) and  $\hat{\lambda}_{\text{opt}}^{(\text{mix})}$  (dashed lines) with various choices of  $m$  for  $K = 5$  (black), 25 (red), and 50 (green).

not already overlap with  $\tilde{p}^{(i)}$ . The total number of possible rematching pairs is  $K(K-1)/2$ , so as  $K$  increases, it is more likely to form additional overlaps.

The advantage of  $\hat{\lambda}_{\alpha}^{(\text{mix})}$  over  $\hat{\lambda}_{\alpha}^{(u)}$  is the inexpensive computational cost in the bridge sampling step,  $T_{\text{BS}}^{(\text{mix})}$ , compared with  $T_{\text{BS}}^{(u)}$  and  $T_{\text{EM}}$ . When  $T_{\text{EM}}$  dominates  $T_{\text{BS}}^{(\text{mix})}$ , typical with large  $K$  (see Figure 17), we can increase  $m$  for the estimator  $\hat{\lambda}_{\alpha}^{(\text{mix})}$  to improve its statistical efficiency without significantly increasing the total computational cost. For easy reference, we use  $\hat{\lambda}_{\alpha}^{(x)}(m)$  to denote the estimator  $\hat{\lambda}_{\alpha}^{(x)}$  with a specific configuration of  $m$ . Figure 17 (left) shows that, for large  $K$ , the differences among the computational cost of  $\hat{\lambda}_{\text{opt}}^{(\text{mix})}$  when  $m = n$  (black dashed line),  $16n$  (red dashed line), and  $32n$  (green dashed line), are negligible compared with  $T_{\text{EM}}$ . The variance of  $\hat{\lambda}_{\text{opt}}^{(\text{mix})}$ , however, drops substantially when  $m$  increases from  $n$  to  $32n$  in Figure 16 (middle). In fact,  $\hat{\lambda}_{\text{opt}}^{(\text{mix})}(16n)$  and  $\hat{\lambda}_{\text{opt}}^{(\text{mix})}(32n)$  are comparable with  $\hat{\lambda}_{\text{opt}}^{(u)}(n)$  in terms of statistical efficiency, but  $\hat{\lambda}_{\text{opt}}^{(u)}(n)$  is much more computationally costly. Consequently,  $\hat{\lambda}_{\text{opt}}^{(\text{mix})}(16n)$  and  $\hat{\lambda}_{\text{opt}}^{(\text{mix})}(32n)$  have larger  $PpS$  than  $\hat{\lambda}_{\text{opt}}^{(u)}(n)$  for moderate and large  $K$ , see Figure 17 (right).

Figure 19 shows that the statistical efficiency of  $\hat{\lambda}_{\text{opt}}^{(u)}$  can also be improved by increasing  $m$ , but the additional computational cost is significant. Therefore, in most cases, the  $PpS$  of  $\hat{\lambda}_{\text{opt}}^{(u)}$  decreases as  $m$  increases. It is, however, important to acknowledge that, for a fixed sample of size  $n$  from  $p$ , the best statistical efficiency achieved by  $\hat{\lambda}_{\text{opt}}^{(u)}$  is better than that of  $\hat{\lambda}_{\text{opt}}^{(\text{mix})}$ , and some of the expensive computational cost of  $\hat{\lambda}_{\text{opt}}^{(u)}$  can be saved by parallel computing, for instance.

To sum up, we recommend using  $L = 50K$  data points from  $p$  to estimate  $\zeta$ . The variance of  $\hat{\lambda}_{\text{opt}}^{(x)}$  can be effectively reduced by increasing  $K$  and/or  $m$  up to certain levels. The rates of reduction in variance are different for  $K$  and  $m$ . When  $K$  is small, increasing  $K$  reduces the variance faster than increasing  $m$ ; when  $K$  is large, increasing  $m$  is more beneficial for reducing the variance. For the estimator  $\hat{\lambda}_{\text{opt}}^{(\text{mix})}$ , having a large  $m$ , e.g.,  $m = 10n$ , is recommended thanks to the inexpensive computational cost  $T_{\text{BS}}^{(\text{mix})}$ .

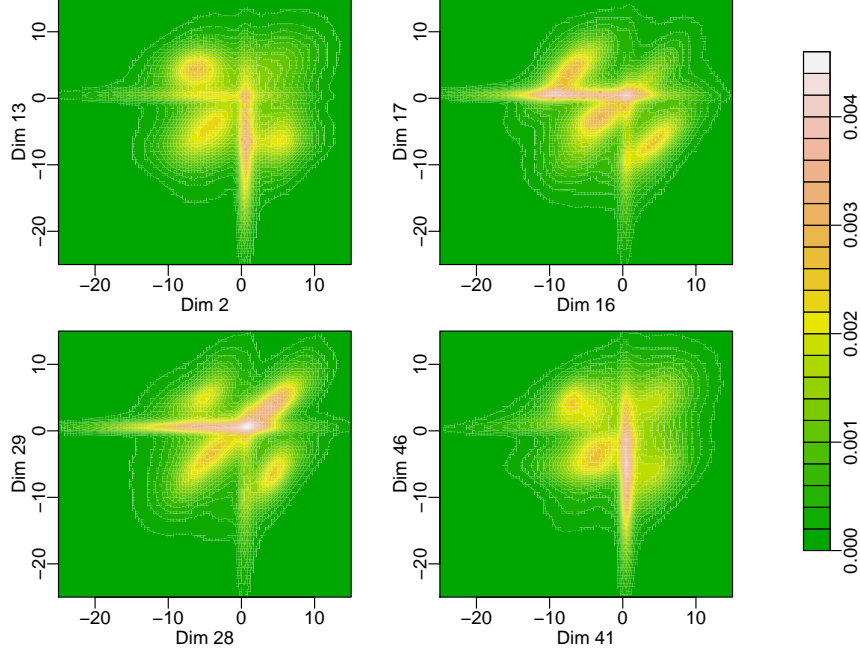


Figure 20: The contours of the density  $p$  projected to different pairs of dimensions.

#### 5.4 Example in 50 Dimensions

Here,  $p$  is a mixture of 30 distributions, including Gaussian distributions,  $t$ -distributions (including Cauchy distributions), and multivariate distributions with gamma and/or exponential marginal distributions and Gaussian copulas. The four 2-D projection contour plots of  $p$  in Figure 20 show the density has very long tails and is quite skewed in some directions. The evaluation of  $p$  is about 700 times more costly than  $\phi$ . The simulation results are based on  $10^4$  replications, and in each replication,  $n = 10^4$  data points from  $p$  are generated.

Figure 21 shows the total computational cost, the RMSE, and the  $PpS$  of  $\hat{\lambda}_{\text{opt}}^{(\mathcal{X})}$ . As in the 10-dimensional example, the RMSE decreases as  $K$  increases up to  $n/100$ , and when  $K > n/100$ , the mixture model overfits the data, resulting in a slight increase in the RMSE of  $\hat{\lambda}_{\text{opt}}^{(\text{mix})}$ . On average,  $\log(\text{RMSE})$  of  $\hat{\lambda}_{\text{opt}}^{(\text{U})}$  is about 60% of that of  $\hat{\lambda}_{\text{opt}}^{(\text{mix})}$ , but the computational cost of  $\hat{\lambda}_{\text{opt}}^{(\text{U})}$  is 4.7 times that of  $T_{\text{opt}}^{(\text{mix})}$ , so in terms of the  $PpS$ ,  $\hat{\lambda}_{\text{opt}}^{(\text{mix})}$  is superior to  $\hat{\lambda}_{\text{opt}}^{(\text{U})}$ . In addition, for large  $K$ , when we increase  $m$  from  $n$  (black lines) to  $16n$  (red) and  $32n$  (green), the total computational cost of  $\hat{\lambda}_{\text{opt}}^{(\text{mix})}$  increases only by a small fraction, but the gain in statistical efficiency is substantial.

Figure 22 shows the impact of increasing  $L/K$  on  $T_{\text{EM}}$  (left),  $T_{\text{opt}}^{(\mathcal{X})}$  (middle), and the  $\log(\text{RMSE})$  (right) of estimators with  $K = 5$  (black lines), 25 (red), and 50 (green). Consistent with Figure 18, as  $L/K$  increases up to 50, the statistical efficiencies of the estimators improve considerably, but as we continue to increase  $L/K$ , the slope of the curves of  $\log(\text{RMSE})$  become very gradual. Hence this example also supports  $L = \min(50K, n/2)$ .

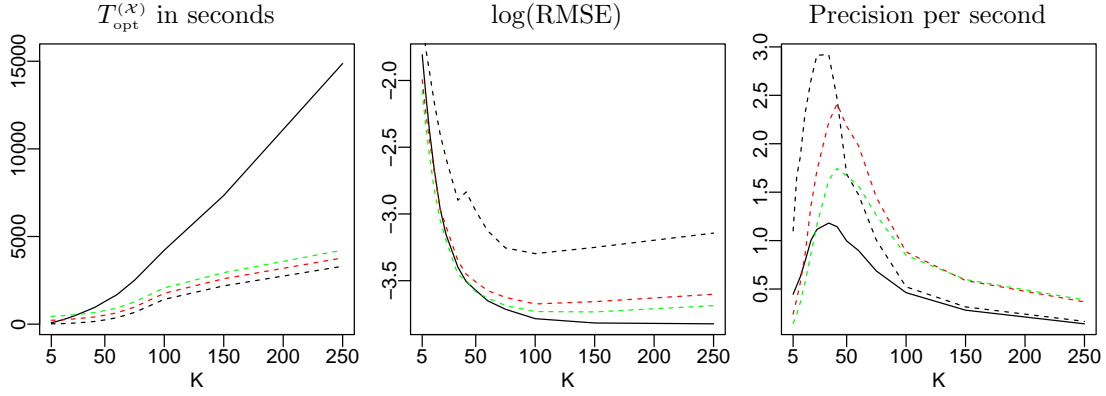


Figure 21: The total computational cost (left), the  $\log(\text{RMSE})$  (middle), and the  $PpS$  (right) of  $\hat{\lambda}_{\text{opt}}^{(U)}$  (solid lines,  $m = n$ ) and  $\hat{\lambda}_{\text{opt}}^{(\text{mix})}$  (dashed lines with  $m = n$  (black),  $16n$  (red), and  $32n$  (green)).

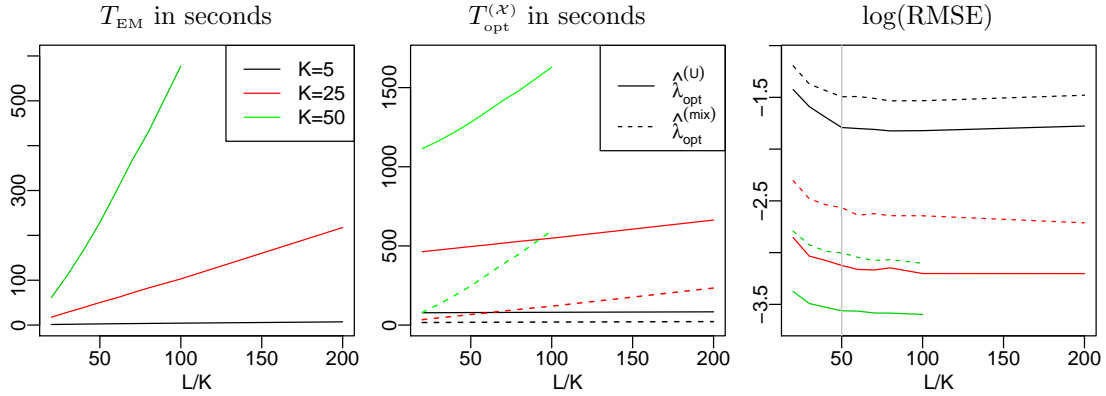


Figure 22: The impact of  $L$  on  $T_{\text{EM}}$  (left),  $T_{\text{opt}}^{(X)}$  (middle), and the RMSE of  $\hat{\lambda}_{\text{opt}}^{(X)}$  (right) in the 50-dimensional example. Black lines:  $K = 5$ ; red:  $K = 25$ ; green:  $K = 50$ . When  $K = 50$ , we can only take  $L/K$  up to 100, because  $L \leq n/2$ .

## 5.5 The Potential of Warp-U for Directly Estimating $c_1/c_2$

So far, we have mainly focused on estimating one normalizing constant, by pairing it with a known constant from  $\phi_{\text{mix}}$ . But in many cases we can also apply the Warp-U strategy directly for estimating the ratio of two unknown normalizing constants. Specifically, suppose we have  $\{w_{i,1}, \dots, w_{i,n_i}\} \stackrel{iid}{\sim} p_i = q_i/c_i$  for  $i = 1, 2$ , and the two densities share the same support. Then the ratio of the two normalizing constants  $c_1$  and  $c_2$  can be estimated by at least three procedures:

1. Estimate  $\lambda_1 = \log(c_1)$  and  $\lambda_2 = \log(c_2)$  separately via Warp-U bridge sampling, denoted as  $\hat{\lambda}_{\alpha, I}^{(U)}$  and  $\hat{\lambda}_{\alpha, II}^{(U)}$ , then  $\lambda = \log(c_1/c_2)$  is estimated by  $\hat{\lambda}_{\alpha, I-II}^{(U)} = \hat{\lambda}_{\alpha, I}^{(U)} - \hat{\lambda}_{\alpha, II}^{(U)}$ .
2. Estimate  $\lambda_1$  and  $\lambda_2$  separately by the algorithm of  $\hat{\lambda}_{\alpha}^{(\text{mix})}$ , denoted as  $\hat{\lambda}_{\alpha, I}^{(\text{mix})}$  and  $\hat{\lambda}_{\alpha, II}^{(\text{mix})}$ , and the corresponding estimator of  $\lambda$  is  $\hat{\lambda}_{\alpha, I-II}^{(\text{mix})} = \hat{\lambda}_{\alpha, I}^{(\text{mix})} - \hat{\lambda}_{\alpha, II}^{(\text{mix})}$ .
3. Estimate the ratio directly by applying bridge sampling to the two sets of Warp-U trans-

formed data.

Here, for (3), we first divide the data  $\{w_{i,1}, \dots, w_{i,n_i}\}$  into two halves, estimate a Gaussian mixture distribution,  $\phi_{\text{mix},i}$ , from the  $L_i (\leq n/2)$  observations of the first half of the data, and then apply the corresponding Warp-U transformation to the second half of the data. Given the calibrated  $\phi_{\text{mix},i}$ , both transformed datasets,  $\{\tilde{w}_{i,j}; j = 1 + \frac{n_i}{2}, \dots, n_i\}$  for  $i = 1, 2$ , have substantial overlap with the common density  $\phi$ , so we expect they overlap with each other substantially. Therefore, we can apply bridge sampling to  $\{\tilde{w}_{i,j}; j = 1 + \frac{n_i}{2}, \dots, n_i\} \stackrel{iid}{\sim} \tilde{q}_i$  for  $i = 1, 2$ , and obtain one estimate of  $\lambda$ , denoted as  $\hat{\lambda}_{\alpha,1}^{(U)*}$ . Reversing the roles of the two halves of the datasets, we obtain a different estimate,  $\hat{\lambda}_{\alpha,2}^{(U)*}$ . The final estimator is  $\hat{\lambda}_{\alpha}^{(U)*} = \frac{1}{2} (\hat{\lambda}_{\alpha,1}^{(U)*} + \hat{\lambda}_{\alpha,2}^{(U)*})$ .

In our simulation to compare these estimators, both  $p_1$  and  $p_2$  are 10-dimensional densities.  $p_1$  is the mixture of 25 multivariate skew- $t$  distributions, as described in Section 4.2, and  $p_2$  is a mixture of 20 multivariate skew- $t$  distributions, which is more spread out than  $p_1$  and has more correlations among different dimensions. The results are based on 5000 replications, and each replication consists of  $n_i = 10^4$  data points simulated from  $p_i$ , for  $i = 1, 2$ . In practice, we can adopt different numbers of components in  $\phi_{\text{mix},1}$  and  $\phi_{\text{mix},2}$ , which define the Warp-U transformations for the two datasets. However, in our simulation, we set  $\phi_{\text{mix},1}$  and  $\phi_{\text{mix},2}$  to have the same number of components  $K$ , and varying  $K$  from 5 to 250.

Figure 23 shows the summary statistics of  $\hat{\lambda}_{\text{opt},\text{I-II}}^{(U)}$ ,  $\hat{\lambda}_{\text{opt},\text{I-II}}^{(\text{mix})}$ , and  $\hat{\lambda}_{\text{opt}}^{(U)*}$  (blue long dashed lines). The difference between the computational cost of  $\hat{\lambda}_{\text{opt}}^{(U)*}$  and  $\hat{\lambda}_{\text{opt},\text{I-II}}^{(U)}$  is that  $\hat{\lambda}_{\text{opt},\text{I-II}}^{(U)}$  involves an additional  $2m$  evaluations of the normal density function, the cost of which is negligible. Interestingly,  $\hat{\lambda}_{\text{opt}}^{(U)*}$  has a much better statistical efficiency than  $\hat{\lambda}_{\text{opt},\text{I-II}}^{(U)}$  or  $\hat{\lambda}_{\text{opt},\text{I-II}}^{(\text{mix})}$ , and the reduction of the RMSE is less affected by the overfitting issue than other estimators for large  $K$ . Figure 23 (right) shows the  $PpS$  of  $\hat{\lambda}_{\text{opt}}^{(U)*}$  is comparable with that of  $\hat{\lambda}_{\text{opt},\text{I-II}}^{(\text{mix})}$  when  $m = 16n$  or  $32n$ . So  $\hat{\lambda}_{\text{opt}}^{(U)*}$  has the advantage of having the lowest RMSE and a competitive  $PpS$ . This simulation study is very limited, but it indicates the potential of  $\hat{\lambda}_{\text{opt}}^{(U)*}$  for estimating normalizing constants.

## 6 Exploring Warp-U Transformations for Sampling

So far our focus has been on applying Warp-U transformations to better use the given draws for estimating normalizing constants. Whereas clearly more work is needed before we can fully realize the potential of Warp-U bridge sampling, we wish to conclude our paper by exploring a different use of Warp-U transformation, that is, for Monte Carlo sampling itself. Specifically, Parno and Marzouk (2014) proposed using transformations from the target distribution to a reference distribution, such as normal, or  $t$ -distribution, to improve the efficiency of a typical Metropolis-Hastings algorithm. Their transformations are deterministic and monotonic maps between the target and the reference distributions. Below we show how to use the stochastic Warp-U transformation to achieve a similar purpose.

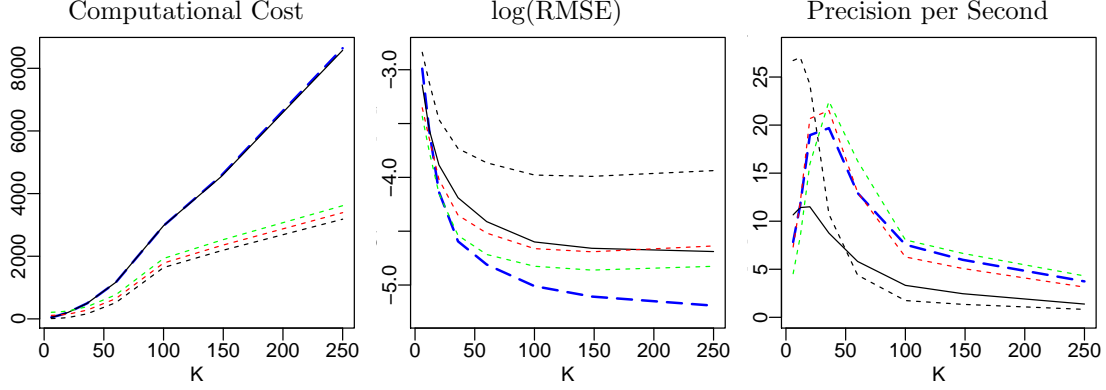


Figure 23: Total computational cost (left),  $\log(\text{RMSE})$  (middle), and  $PpS$  (right) of  $\hat{\lambda}_{\text{opt},\text{I-II}}^{(U)}$  (solid lines,  $m = n$ ),  $\hat{\lambda}_{\text{opt},\text{I-II}}^{(\text{mix})}$  with  $m = n$  (dashed black lines),  $16n$  (dashed red lines), and  $32n$  (dashed green lines), and  $\hat{\lambda}_{\text{opt}}^{(U)*}$  (blue long dashed lines).

Specifically, going back to Figure 5, we see how  $W \sim p$  is transformed to  $\widetilde{W} \sim \widetilde{p}$  through Warp-U transformation. Obviously we can reverse this transformation. First, for each sampled  $\widetilde{w} = \mathcal{F}_\psi(w) \sim \widetilde{p}$ , we draw a new  $\psi^*$  from the conditional distribution of  $\Psi$  given  $\widetilde{W} = \widetilde{w}$ , which can be obtained via (c.f. (17) for notation)

$$p_{\Psi|\widetilde{w}}(\psi|\widetilde{w}) \propto p_{\Psi,\widetilde{w}}(\psi,\widetilde{w}) = p_{\Psi,w}(\psi,\mathcal{H}_\psi(\widetilde{w}))|\mathcal{H}'_\psi(\widetilde{w})| = \varpi(\psi|\mathcal{H}_\psi(\widetilde{w}))p(\mathcal{H}_\psi(\widetilde{w}))|\mathcal{H}'_\psi(\widetilde{w})|, \quad (29)$$

where  $\mathcal{H}_\psi = \mathcal{F}_\psi^{-1}$ , as before. This sampling is typically easy, especially when we choose  $\Psi$  to be discrete, because the right-hand side of (29) is readily available from our construction of  $\Psi$  and the map  $\mathcal{F}_\Psi$ , and from our ability to evaluate the (unnormalized) target density  $q \propto p$ . We then apply the inverse transformation to  $\widetilde{w}$  to obtain  $w^* = \mathcal{H}_{\psi^*}(\widetilde{w})$ . But because  $w = \mathcal{F}_\psi^{-1}(\widetilde{w}) = \mathcal{H}_\psi(\widetilde{w})$ , we see that  $w^*$  and  $w$  have identical distribution since  $\psi^*$  and  $\psi$  are two *independent* draws from the same conditional distribution (29), by our very construction. That is, the process moving from  $w$  to  $w^*$  preserves the target distribution  $p$ , hence repeating it will yield a Markov chain with  $p$  as its stationary distribution:

$$w^{(t+1)} = \mathcal{H}_{\psi^*}(\mathcal{F}_\psi(w^{(t)})), \quad t = 1, 2, \dots \quad (30)$$

Furthermore, because  $w^{(t+1)}$  and  $w^{(t)}$  are conditionally independent given  $\widetilde{w}$ , with judicious choices of the transformation of  $\mathcal{F}_\psi$  (and hence its inverse  $\mathcal{H}_\psi$ ) that reduce the dependence of (29) on  $\widetilde{w}$ , we can improve the convergence speed of the resulting chain.

As a proof of concept, we use a mixture of 3 bivariate skewed- $t$  distributions as our target  $p$ , to explain and demonstrate how a Warp-U transformation can help our chain to mix fast. We use three different  $\phi_{\text{mix}}(\omega)$ , in the form of (9), with  $K = 5, 10, 20$  respectively to determine the Warp-U transformation. See Figure 24 for the contour plots of  $p$  (left), and  $\phi_{\text{mix}}$  when  $K = 5$  and 10, which are obtained by fitting (9) to  $10^4$  samples from  $p$ . In real applications, of

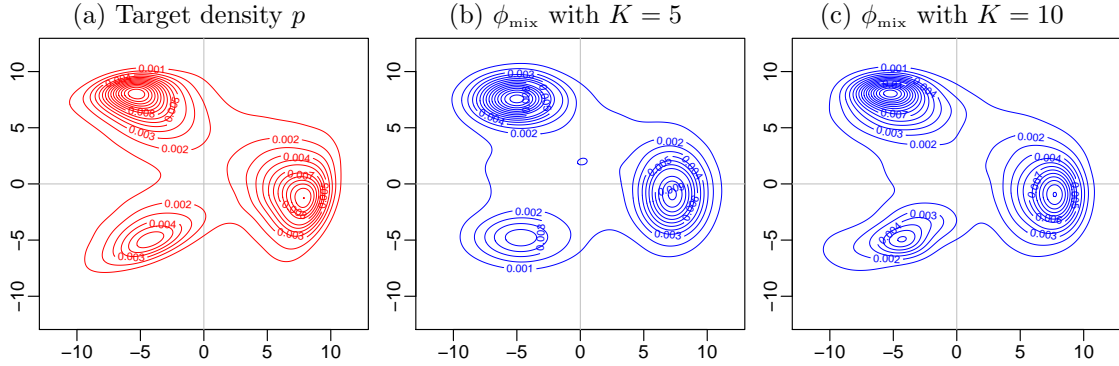


Figure 24: (a) contour plot of the 2-D target density  $p$ , a mixture of 3 skewed- $t$  distributions, (b) and (c) contour plots of  $\phi_{\text{mix}}$  used for determine the Warp-U transformation with  $K = 5$  and  $K = 10$ .

course, one will not have such samples before implementing a reliable MCMC algorithm. For our simulation study, we use such samples fitted deliberately to wrong models to mimic the different constructions of  $\phi_{\text{mix}}$  based on prior information of varying qualities, as in real applications. Here all mixture normal models are very wrong in terms of both the number of mixture components (which is 3 for the target density  $p$ ) and the distribution shapes (which are *skewed t* for  $p$ ). Our goal here is not to estimate  $p$  well (after all, we know  $p$  completely), but rather to create a convenient approximation that has a significant overlap with  $p$ .

Once the Warp-U transformation  $\mathcal{F}_\psi$  is formulated, we start initially with  $w^{(0)} = (0, 0)$ , and then apply (30) to compute  $w^{(t+1)}$ , for  $t = 1, 2, \dots, 10^3$ . The 2-D scatter plots in the left column of Figure 25 show the samples we make with different Warp-U transformations characterized by different  $\phi_{\text{mix}}$ 's. The corresponding histograms for the sum of the two coordinates (as a convenient illustration), i.e.,  $w_s^{(t)} = w_1^{(t)} + w_2^{(t)}$ , are given in the middle column, where the red curves are the target distribution of  $W_s = W_1 + W_2$  multiplied by some constants (to match the scale of the histogram). The plots in the right column are the corresponding auto-correlation and trace plot of  $w_s^{(t)}$ .

When the number of components in  $\phi_{\text{mix}}$  is small, i.e.,  $K = 5$ ,  $\phi_{\text{mix}}$  is quite different from  $p$ . The resulting poor stochastic map is unable to efficiently explore the whole space. Although we ran for  $10^3$  iterations, the chain was only able to reach 86 unique values. However, the auto-correlation of these draws is very small. From the trace plot, we also see that the chain was able to move among the dense areas of  $p$  frequently. This is not surprising considering the random (but stationary) movement induced by (30), a general strategy to prevent a Markov chain from becoming trapped. As  $K$  increases, the quality of our Warp-U sampler improves, again confirming our intuition that the effectiveness of Warp-U sampling depends on the quality of the Warp-U transformations, indexed here by  $K$ . When  $K = 20$ , the ACF plot suggests that the chain almost delivers i.i.d. draws. This potential can also be understood from the trivial



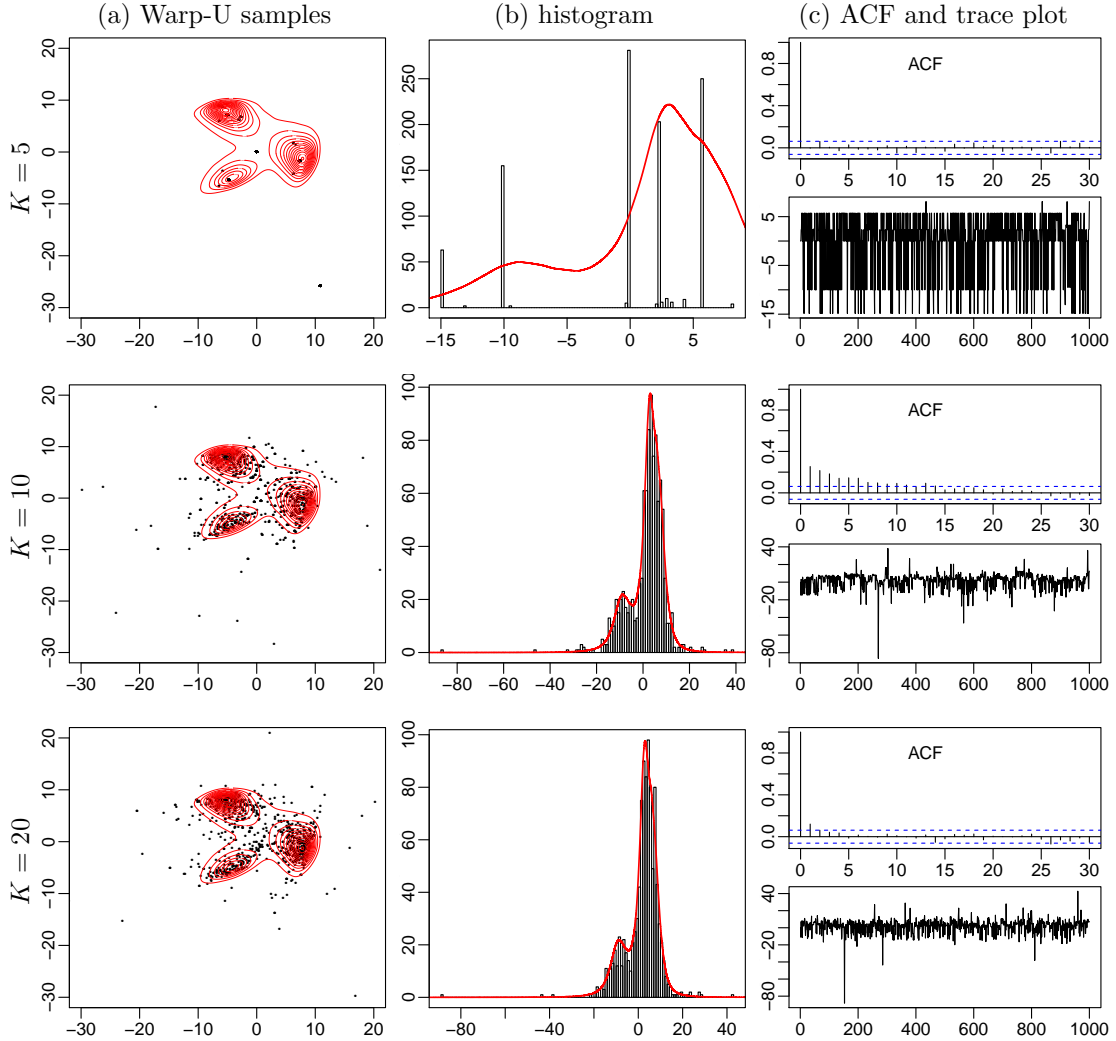


Figure 25: (a) scatter plots of samples from Warp-U transformations determined by different  $\phi_{\text{mix}}$ 's with the number of components varying from  $K = 5$  (top), 10 (middle), to 20 (bottom); (b) histograms of the sum of the two coordinates  $w_s^{(t)} = w_1^{(t)} + w_2^{(t)}$ ; the red curves are the density of  $W_s = W_1 + W_2$  multiplied by some constants (to match the scale of the histogram); (c) auto-correlation and trace plot of  $w_s^{(t)}$ .

case when  $\phi_{\text{mix}} = p$ , that is, when we have perfect information to “decompose”  $p$ . In such cases, the Markov chain defined by (30) would lead to an i.i.d. sequence because  $P_{\Psi|\tilde{w}}(\Psi = k|\tilde{w}) = \pi_k$ , that is, (29), is free of  $\tilde{w}$ . This suggests that the closer we are able to match  $\phi_{\text{mix}}$  to the target  $p$ , the more likely we would have a fast mixing chain.

We emphasize that the chain (30) can be constructed on top of any Markov chain, because it builds on an augmented space  $(W, \Psi)$ , and uses (typically discrete)  $\Psi$  to move among different regions, which do not need to correspond to any actual modal areas of the target, as far as the

validity of the chain goes. However, there is no free lunch. How effective this strategy is will depend critically on how much we know about  $p$ , to construct a sensible “moving index”  $\psi$  that will help to capture the major mass areas of  $p$ . We will explore these issues in our applied work, and we invite others to try this Warp-U strategy in their applications, as it is both flexible and easy to implement.

In a nutshell, we believe Warp-U transformations and, more generally, stochastic transformations have much to offer for efficiently analyzing as well as generating Monte Carlo samples. We therefore hope our paper can serve as a stimulus to encourage more researchers to explore this stochastic land of opportunities, which is likely to be far more vast than currently realized.

## References

- Ali, S. M. and S. D. Silvey (1966). A general class of coefficients of divergence of one distribution from another. *Journal of the Royal Statistical Society. Series B (Methodological)* 28, 131–142.
- Alspach, D. L. and H. W. Sorenson (1972). Nonlinear Bayesian estimation using Gaussian sum approximations. *IEEE Transactions on Automatic Control* 17(4), 439–448.
- Azzalini, A. (2011). R package sn: The skew-normal and skew-t distributions (version 0.4-17). URL <http://azzalini.stat.unipd.it/SN> 20.
- Azzalini, A. (2013). *The skew-normal and related families*. Cambridge University Press, New York.
- Bennett, C. H. (1976). Efficient estimation of free energy differences from Monte Carlo data. *Journal of Computational Physics* 22(2), 245–268.
- Bornkamp, B. (2011). Approximating probability densities by iterated Laplace approximations. *Journal of Computational and Graphical Statistics* 20(3), 656–669.
- Ceperley, D. M. (1995). Path integrals in the theory of condensed helium. *Reviews of Modern Physics* 67(2), 279–355.
- Chen, J. and X. Tan (2009). Inference for multivariate normal mixtures. *Journal of Multivariate Analysis* 100(7), 1367–1383.
- Chen, J., X. Tan, and R. Zhang (2008). Inference for normal mixtures in mean and variance. *Statistica Sinica* 18(2), 443–465.
- Day, N. E. (1969). Estimating the components of a mixture of normal distributions. *Biometrika* 56(3), 463–474.

- Gelman, A., J. B. Carlin, H. S. Stern, D. B. Dunson, A. Vehtari, and D. B. Rubin (2013). *Bayesian data analysis*. CRC Press, Boca Raton.
- Gelman, A. and X.-L. Meng (1998). Simulating normalizing constants: From importance sampling to bridge sampling to path sampling. *Statistical Science* 13, 163–185.
- Kiefer, J. and J. Wolfowitz (1956). Consistency of the maximum likelihood estimator in the presence of infinitely many incidental parameters. *The Annals of Mathematical Statistics* 27, 887–906.
- Kong, A., P. McCullagh, X.-L. Meng, D. Nicolae, and Z. Tan (2003). A theory of statistical models for Monte Carlo integration (with discussions). *Journal of the Royal Statistical Society: Series B (Statistical Methodology)* 65(3), 585–604.
- Meng, X.-L. and S. Schilling (2002). Warp bridge sampling. *Journal of Computational and Graphical Statistics* 11(3), 552–586.
- Meng, X.-L. and W. H. Wong (1996). Simulating ratios of normalizing constants via a simple identity: A theoretical exploration. *Statistica Sinica* 6(4), 831–860.
- Parno, M. and Y. Marzouk (2014). Transport map accelerated Markov chain Monte Carlo. *arXiv preprint arXiv:1412.5492*.
- Shao, Q.-M. and J. G. Ibrahim (2000). *Monte Carlo methods in Bayesian computation*. Springer Series in Statistics, New York.
- Tan, Z. (2013). Calibrated path sampling and stepwise bridge sampling. *Journal of Statistical Planning and Inference* 143(4), 675–690.
- Voter, A. F. and J. D. Doll (1985). Dynamical corrections to transition state theory for multistate systems: Surface self-diffusion in the rare-event regime. *The Journal of Chemical Physics* 82(1), 80–92.